Review of the paper entitled
"Large-eddy simulation of radiation fog with comprehensive two-moment bulk microphysics: impact of different aerosol activation and condensation parameterizations"

by Johannes Schwenkel and Bjorn Maronga

RC1: This paper addresses the difficult topic to evaluate the influence of cloud microphysical parameterizations on large-eddy simulation of radiation fog. The results are based on one case of deep fog observed at Cabauw (Netherlands). The subject of the manuscript is interesting as radiation fogs are not well known, and particularly the influence of microphysical processes on the fog life cycle. However, I think that some revisions will be helpful to make this paper clearest.

Author's answer: First of all, we would like to thank the reviewer for the detailed and constructive feedback. In particular, the suggestions on the visibility and time marks of the fog cycle were added and are now discussed in the revised manuscript. Furthermore, the other points of criticism regarding the aerosol concentration and the difference between shallow fog and deep fog were taken into account and the manuscript was adapted accordingly. With the help of these comments, it was possible to contribute to a significant improvement in the work and to clarify the research.

RC1: 1. clarify the effect of microphysical parameterizations on the fog life cycle :
Following Fig. 8, the microphysical parameterizations used do not modify the fog onset, the time when fog becomes optically thick, the lifting time of fog and the time when fog is completely dissipated. However, it is very difficult to evaluate precisely these parameters from Fig. 8. I think that a table summarizing these 4 times, crucial in the fog life cycle (onset, transition into optically thick fog, lifting time and complete dissipation), would be helpful to evaluate the impact of the parameterizations used. Could you please add this table and discuss the impact of microphysical parameterizations on these parameters? Please elaborate.
Author's answer: We agree with this objection that a table is the method of choice for displaying these parameters. In the revised manuscript the table is provided in section 4.3 and discussed in the following.
Modification(p19, l1): The effect of the different activation schemes on the time of the fog life cycle is summarized in Tab. 2. The largest differences occur for simulation N2EXP in comparison to N1EXP and N3EXP. The onset is delayed by 25 min, while the maximum liquid water mixing ratio is reached 45 min earlier, than in the other cases. Also lifting and dissipation are affected and occurred15 min and 40 min (with respect to simulation N3EXP) earlier. This is due to a lesser absolute liquid water mixing ratio which is more easily evaporated by the incoming solar radiation. Therefore, it can be concluded that the use of different activation schemes (if they change the droplet number concentration) has an effect on the time marks on the life cycle, even though the general shape stays untouched

RC1: 2. effect of microphysical parameterizations on visibility at ground level :
Your simulations demonstrate that the microphysical parameterizations mainly impact the microphysical properties of the fog layer (liquid water mixing ratio and LWP). These parameters (ql and nc) have a significant impact on the diagnosed visibility. Could you please discuss the impact of the microphysical parameterizations used on the diagnosed visibility at ground level? Is this impact significant? Or is this impact of the same magnitude than uncertainties due to visibility diagnostic? Please elaborate.
Author's answer: This is a good suggestion, since the visibility was a measured quantity during CESAR. We have added time series of the simulated and measured visibility (even though it was not our aim to represent a specific fog case as close as possible to observations) in the revised version.

Modification(p2, l2): In Fig. 9 the simulated visibility for the cases N1-N3 in 2 m height as well as the observed value is shown. For the simulation the visibility is calculated by
$vis=1002/(n_c \rho q_l)^{0.6473}$,
following Gultepe et al. (2006). Here, n_c and q_l must be given in units of cm^{-3} and gm^{-3}, respectively. Hence, the visibility is significantly affected by the droplet number concentration and the liquid water content. As one can see all simulations reproduce the general trend of the visibility quite well. During the onset of the fog all simulation tend to underestimate the visibility. In the mature phase Simulation N2 exhibit the largest values to the observed visibility, but matches best during the lifting phase. However, it should be mentioned that it was not our goal to mimic one particular fog case.

RC1: **3. effect of aerosol :**
Your tests are done for a background aerosol concentration of 842cm−3 and for a given aerosol chemical composition. What is the impact of this hypothesis on your results? Are your results also valid in a highly polluted atmosphere (e.g. observation made during WIFEX), or in an atmosphere with low aerosol concentration? Please elaborate.
Author's answer: It is true, that our simulations shows results for only one aerosol environment. However, these are well-known and frequently investigated conditions. Furthermore, in many of the observed radiation fog events the underlying conditions are similar the chosen aerosol conditions of this study.
Of course, changed aerosol conditions would change the absolute numbers of the errors done with the investigated microphysical parametrizations. However, the qualitative findings will be untouched. The reason why we have not conducted simulations for only quantifying the difference for different aerosol environments is then based on the needed computational resources which are tremendous (54h on 3072 computer cores).
However, we agree that these findings with their concrete numbers are limited to cases with continental aerosol conditions. Due to that we have adapted the manuscript to clarify that it's based on continental aerosol conditions.
Modification(different passages): [..] continental aerosol conditions [..]

RC1: 4. **shallow fog / deep fog**
Are your findings also true for shallow fog (with thermal inversion at ground level)? The dynamical processes between shallow and deep (mature) fog are strongly different. And consequently, the impact of microphysical parameterizations could be very different during the fog life cycle (due to difference in supersaturation magnitude). Could you please clarify the sensitivity of microphysical parameterizations depending on the fog type (ie shallow vs deep fog)?
Author's answer: This is an interesting objection. However, in current research the focus is more on deep fog events, as these affect our everyday life much more (e.g. dangers for air and car traffic). Moreover, even though the dynamics of shallow fog compared to a deep fog event might be different, it was not our aim to derive universally valid statements for the entire parameter space (as for different aerosol conditions).
Unfortunately, as stated in the previous comment this is with a high-resolved (isotropic grid-spacing of 1m) LES not possible where one simulation requires many computer resources (as mentioned above).
Form the fundamental research point of view, different microphysical parameterizations might also affect shallow fog since the crucial parameter is the supersaturation.
But we agree, to clarify that our statements are especially valid for a deep fog case under typical continental aerosol conditions, and according to that we had adapted our manuscript.
Modification(at different passages): [..] deep [..]

RC1: 5. Stolaki et al. (2015) use 1D model. She does not use 2D LES. Please modify (p2 l2).
Author's answer: This is right. It is corrected in the revised revision.

Modification(p2, l2): [..] while using the one-dimensional mode of the MESO-NH model [..]

RC1: 6. Figure 6b, 6c, 6d, 9c and 10c are very hard to read (too many curves on the same plot). Could you please try to improve these figures?
Author's answer: As also the other reviewer criticized the figures. We modified them, as we separate them to more individual plots.
Modification(Fig 6,9,10): We modified the figures 6,9 10.

Review of the paper acp-2018-1139 « Large-eddy simulation of radiation fog with comprehensive two-moment bulk microphysics: Impact of different aerosol activation and condensation parameterizations» from Johannes Schwenkel and Björn Maronga

RC2: The manuscript presents a study of condensation and activation parametrizations for a LES of radiation fog. This is an interesting topic as most of LES of fog now use 2-moment microphysical schemes and also produce an overestimation of cloud concentration and mass. Therefore these questions of activation are central. The relevance of saturation adjustment for LES has been raised by Thouron et al. (2012) for stratocumulus and Lebo et al. (2012) for deep convective clouds. Since these studies, it is the first time that this question is dealing with fog. So this study could be an original contribution to the modelling community.
But the study suffers from a lot of weaknesses and is not convincing. Therefore it misses the objective. Whilst the topic is interesting, and could be ultimately worthy of publication, I feel major modifications to the manuscript are required, and substantial inputs are necessary before publication.

Author's answer: First of all, we would like to thank the reviewer for the detailed and constructive feedback. Especially the high expert competence of the review allowed us to overcome the weaknesses, to extend the study by reasonable points and to focus the scientific result.

RC2: The case is an observed fog event, but you never show observation so there is no reference. Therefore you cannot say that liquid water content is overestimated in some configuration.
Author's answer: Indeed, the simulated fog case was an observed event during CESAR. A detailed comparison to measurements is given in Maronga and Bosveld, 2017. However, the relevant (in terms of our study needed) quantities, such as droplet number concentration, liquid water mixing ratios and liquid water path were not measured. In our statements, which claim an overestimation of certain configurations, we therefore refer to theoretical considerations.
However, we agree that in some passages that this was not clear enough or not sufficiently proved. Thus, we modified those passages and only make valuations were there are justified.
Modification(p2, l2): Rewrite passages, which claimed an overestimation and could not be sufficiently proved.

RC2: You draw conclusions with only one case. For instance 6.9 % just corresponds to one case and you generalize this result to characterize the impact of adjustment saturation for fog (in the abstract/conclusion). In the same way, for the sensitivity of the time step, you claim that you test a larger time step without showing the result, and you state that the effect is not negligible. This is not scientific and admissible. A broad range of time steps needs to be compared. Additionally, what is the sensitivity to the spatial resolution?
Author's answer: We agree with you general objection that drawing quantitative conclusions by two simulations is not admissible. Due to that we removed the passages were we generalized our results. Further, we labeled our results as that was they are: Findings from high-resolved LES study with (typical) continental aerosol conditions. From that we can only conclude that similar cases might show a similar trend but may differ in their concrete numbers. Moreover, as you suggested in the next comment we added a prognostic approach for simulating supersaturation. Due to carefully double checking we noted a bug in our model code and must repeat one simulation (old C1, renamed in EXP in the revised manuscript). Accordingly, the quantitative results changed but the general qualitative findings remain untouched.
Furthermore, we removed the conclusion that differences getting smaller by a larger time-step, as it was not sufficiently proved and mixed with a comparison to simulations with a different grid-

spacing. Therefore. the effect was not isolated to the time step.
Due to computational costs (one simulation requires approximately 48h on 3072 cores on a supercomputer) a broad range of time steps could not be conducted with this setup, since only (due to dynamical stability reasons) a reduction of the time-step is allowed.
However, we added a sensitivity study with a spatial resolution of 4m and 2m in chapter 4.4 as there changes to the grid-spacing should have the strongest effect.
Modification(chapter 4.2 and 4.4): As this referee comment involve major modifications we kindly refer to the revised manuscript and the attached manuscript, which highlights all changes in comparison to the first version individually.

RC2: The objective to evaluate the impact of saturation adjustment was promising but disappointing as you do not compare explicit vs saturation adjustment for 2 moment microphysical scheme, despite the fact that 2 moment microphysical schemes are the most frequently used in LES of fog. At least a N0 test with Twomey or Cohard and saturation adjustment needs to be added, to be compared to N1 or N2. Moreover a more complete study of this topic would include a pseudo-prognostic approach of supersaturation (Thouron et al., 2012).
Author's answer: We decided to follow the reviewer suggestion and added three more high-resolved simulations.
Firstly, we extended the part of the study where the influence of different condensational growth parameterizations are isolated and investigated (in terms of using a 1D-microphysics with fixed number concentration). Here, we also added a prognostic approach for calculating the supersaturation, which drives the strength of the diffusional growth.
Secondly, as the reviewer proposed we added the saturation adjustment case with a activation scheme of Cohard et al., 1998. Moreover, we also applied the same activation scheme by using the prognostic approach for calculating supersaturation. By doing so, we introduced (following Thouron et al., 2012.) a new section where the influence and feedback of different supersaturation calculation on the droplet activation (by using the scheme of Cohard et al., 1998) is discussed.
For that we compared N2EXP to the new simulations N2SAT and N2PRG. The new introduced simulations are summarized in the Table (bold marked). Note, that though these major modifications we decided to rename the simulation to make it more intuitively.

#	Simulation	Activation Scheme	Nc	Na	Condensation Scheme
1	SAT	None	150	none	Saturation adjustment
2	EXP	None	150	none	explicit
3	**PRG**	**None**	**150**	**none**	**prognostic**
4	N1EXP	Twomey	Not fixed	842	explicit
5	N2EXP	Cohard et al	Not fixed	842	explicit
6	N3EXP	Khvorostyanov and Curry (2006)	Not fixed	842	explicit
7	**N2SAT**	**Cohard et al.**	**Not fixed**	**842**	**Saturation adjustment**
8	**N2PRG**	**Cohard et al.**	**Not fixed**	**842**	**Prognostic**

Modification(chapter 2.2.2 and chapter 4.4): [..] As this referee comment involve major modifications we kindly refer to the revised manuscript and the attached manuscript, which highlights all changes in comparison to the first version individually

RC2: The comparison of different activation parametrizations (4.3) is reduced to a sensitivity test to the CCN concentration, and contributes nothing new. Why have you not chosen more equivalent activation properties, for instance if the 3 curves pass by the same point S=0.1 % NCCN=100 cm-3 (Fig.A1) in order to compare the 3 parametrizations ? Because the 3 activation schemes present different curvatures according to S, and this point is not discussed.
Author's answer: Our idea here was to show the differences between different activation schemes initializing in such a way (by using the in literature described values, see Cohard et al., 1998, Khvorostyanov and Curry, 2006 and Pruppacher et al., 1998 (chapter 2.2)) that they are describing the same aerosol environment. So basically we didn't change the aerosol concentration, since we leaved this parameter untouched.
However, considering the activation spectra displayed in A1 we agree that there is mainly a offset between the schemes of Cohard et al., 1998 and Khvorostyanov and Curry, 2006. In contrast to that to the Twomey-scheme we see both, an offset as well as a different curvature. As you suggest we could modify the activation spectrum (or more precisely the parameter describing the aerosol environment) in a such a way that they pass by the same point. But again, the overall goal was more from the view of a users, which is maybe interested in which total differences can be produced by using this or that scheme. As this get not clear enough in the first version of the manuscript, we modified the revised version accordingly.
Modification(Chapter 1): [..]

RC2: There are a lot of inaccuracies. More specifically:

RC2(1): The introduction has been neglected and does not raise the scientific questions. The fact that most of LES of fogs produce an overestimation of cloud concentration and mass is one argument to justify this study (See Mazoyer et al., 2017).
Author's answer: After major modifications also the introduction was carefully revised. Furthermore, the study of Mazoyer et al., 2017 was added. But more important, the missing scientific question was clarified.
Modification(Chapter 1): [..] As Mazoyer et al. (2017) and Boutle et al. (2018) stated that both, LES and NWP models tend to overestimate the liquid water content and the droplet number concentration for radiation fog the following questions are derived from these shortcomings:
(i) Is saturation adjustment appropriate as it crucially violates the assumption of equilibrium? How large is the effect of different supersaturation calculations on diffusional growth?

(ii) What is the impact of different activation schemes on the fog life cycle for a given aerosol environment?

(iii) As the number of activated droplets is essentially determined by the supersaturation, how large is the effect of different supersaturation modeling approaches on aerosol activation and therewith on the strength and life cycle of radiation fog (cf. Thouron et al., 2012)?

In the present paper we will try to answer these questions employing high-resolution LESs based on an observed typical deep fog event with continental aerosol conditions. The paper is organized as follows: Section 2 outlines the methods used, that is the LES modeling framework and the microphysics parameterizations used. Section 3 provide an overview of the simulated cases and model setup, while results are presented in Section 4. Conclusions are given in Section 5.

RC2(2): p2 : Stolaki et al. (2015) used 1D simulations
Author's answer: This is right. It is corrected in the revised revision.
Modification(p2, l2): [..] while using the one-dimensional mode of the MESO-NH model [..]

RC2(3): p2 l 7 : What is Salsa? Reference?
Author's answer: That was right, an complete reference was missing. SALSA is a sectional module for a size resolved treating for aerosols.
Modification(p2, l7): [..] Sectional Aerosol module for Large Scale Applications (SALSA) (Kokkola et al.,2008) [..]

RC2(4): p 2 l 11 : Mazoyer et al. (2017) needs to be added
Author's answer: Added in the revised manuscript.
Modification(p2, l8): [..]Mazoyer et al., 2017 conducted similar to Stolaki et al., 2015 simulation of the ParisFog with the MESO-NH model but using the 3D-LES mode, and focusing on the influence of drag effect on droplet deposition

RC2(5): p 2 l 20 : Thouron et al. (2012) is the first paper raising the question of how relevant the saturation adjustment is for LES of clouds. The paper draws extensively on Thouron et al. (2012) but it is not sufficiently referenced in different parts.
Author's answer: We agree, and have added this reference in the missing passages.
Modification(p?, l?): e.g. p2, l30, p7,l3, p8, l6

RC2(6): p2 l31 : What does revision 2675 mean?
Author's answer: Our LES-model PALM is maintained with the trac-system. Due to that every change in the model code or corresponding files is explicitly identified with the revision number. With that number it is also possible to get the for this studies used model code from our web page, which is mentioned in the acknowledgments.
Modification(p2, l31): None**.**

RC2:(7): p 3 : some information about PALM is missing : What are the numerical schemes used? Is the turbulence scheme 1D or 3D (does it parametrize horizontal turbulent fluxes)? More important : what are the parametrizations for the computation of cloud optical properties?
Author's answer: We have added the missing information about PALM and how optical properties of clouds and how they are treated in the radiation model. By doing so we were as short as possible to avoid to lengthen the manuscript, but more important as precise as necessary.
Modification(p3-4): [..] PALM is discretized in space using finite differences on a Cartesian grid. For the non resolved eddies a 1.5-order flux-gradient subgrid closure scheme after Deardorff (1980) is applied, which includes the solution of an additional prognostic equation for the subgrid-scale TKE. Moreover, the discretization for space and time is done by a fifth-order advection scheme after Wicker and Skamarock (2002) and a third-order Runge-Kutta time-step scheme (Williamson, 1980), respectively. The interested reader is referred to Maronga et al., 2015 for a detailed description of the PALM model.

[..]This favors an improved calculation of the effective radius, which is calculated by

$$r_{eff} = \frac{3 q_l \rho}{4 \pi n_c \rho_l}^{1/3} \exp(\log(\sigma_g)^2),$$

where q_l is the liquid water mixing ratio, rho the air density, ρ_l being density of water and σ_g=1.3 the geometric standard deviation of the droplet distribution. The effective radius is the main interface between the optical properties of the cloud and the radiation model RRTMG. Note, that 3D radiation effects of the cloud are not implemented in this approach, which however could affect the lateral edges.

RC2(8): p 7: The explicit supersaturation calculation corresponds to the scheme B in Thouron et al. (2012) (diagnostic of supersaturation). They have shown that this method is very sensitive

to small errors in temperature and mixing ratio. Spurious values of supersaturation have a significant impact on CCN activation. They showed that it also overestimates CCN activation at the top. All this information should be recalled as well as the reference.
Author's answer: We agree, and added a prognostic approach for treating supersaturation to our work. This includes a new chapter discussing the effect of different methods for supersaturation calculation on CCN activation.
Modification(chapter 2.2.2 and chapter 4.4): [..] As this referee comment involve major modifications we kindly refer to the revised manuscript and the attached manuscript, which highlights all changes in comparison to the first version individually.

RC2(9): P7 line 15-17 is not clear. Could you improve the explanation if you want to justify that a pseudo-prognostic approach is not interesting or necessary.
Author's answer: Our primary reasons for not using a prognostic approach for solving the supersaturation was that a small grid spacing is the method of choice to migitate the error introduced by spurious cloud edge supersaturations (e.g. Hoffmann, 2016). As we already used this lowest feasible grid-spacing for simulating such a case (simulating this fog event with Δ=1m occupies 3072 processor units for approximately 48h on a supercomputer).
However, since spurious supersaturations also occur for small grid spacing's since it is more a question of the ratio of advection and condensational phase relaxation time scales we decided to implement and test this method in our model and include the results within this manuscript.
Modification(chapter 2.2.2 and chapter 4.4): [..] As this referee comment involve major modifications we kindly refer to the revised manuscript and the attached manuscript, which highlights all changes in comparison to the first version individually.

RC2(10): Tab 1 and Part 4 : please add and analyze a new test N0 with Twomey or Cohard and saturation adjustment.
Author's answer: We added and analyzed a case with saturation adjustment and the activation scheme of Cohard et al., 1998. Moreover, we also added a case using the prognostic approach by using the same activation scheme. This involves a new chapter, describing the feedback of different supersaturation calculation methods on droplet activation similar to Thouron et al, 2012.
Modification(chapter 2.2.2 and chapter 4.4): [..] As this referee comment involve major modifications we kindly refer to the revised manuscript and the attached manuscript, which highlights all changes in comparison to the first version individually.

RC2(11): Fig 3 : you say « height averaged » and then 2m and 20m. So what?
Author's answer: We agree that this description was wrong. It is a horizontal average at different heights.
Modification(Fig. 3): Time series of horizontal [..]

RC2(12): Fig.4 : do time marks refer to C1 or REF?
Author's answer: Due to major modification's of the manuscript this passages is removed.
Modification(p?, l?): [..]

RC2(13):P11 l 4 : why are the time steps in the plural? Can you also explain shortly why they are so small?
Author's answer: The revised version uses the singular. During the time integration the time step is calculated dynamically. For calculating the length of the new time step our model consider the CFL-criterion (Courant et al., 1928) as well as the diffusion-criterion (e.g. Jacobson, 2005, chap 6.4.4.1)

and afterward takes the minimum of both. Both of them led to a decreased time step by decreasing grid spacing and increasing wind speed. In our cases the grid spacing is relatively small with some moderate wind speed. We had to use a case where the wind speed is strong enough to generate turbulence, otherwise our LES were not able to simulate such a case, which then can favorably be done by DNS.
Modification(p?, l?): [..] time step [..]

RC2(14):P 12 l 17 : it is C1 minus REF, isn't it?
Author's answer: Yes, it is. However, due to major modifications part is removed from the revised manuscript.

RC2(15):P12 l 21-22 : How are these higher liquid mixing ratios produced?
Author's answer: This is explained by smaller evaporation rates in the case of C1. Due to that the case C1 exhibits in higher levels during the lifting phase of the fog slightly larger values for the liquid water mixing ratio, as evaporation is the dominant process.
Modification(p?, l?): [..]as evaporation is the dominant process during the dissipation phase.

RC2(16):P 12 l 27 : Again why is the time step approximated?
Author's answer: Again, the time step is not fixed. Instead it is calculated new at every time step. Therefore, there is no constant value during one simulation, instead if it is set manually. The latter should only be done if one is sure that the aforementioned criterion are not violated by the manual set time step. But I agree that 'approximately' is the wrong term to describe a well known value. Instead I calculated the average time step of a 4m simulation which was 0.58 s.
Modification(p12, l7): [..] on average 0.58 [..]

RC2(17):P12 l 26-35 : This paragraph is not acceptable as you conclude on a sensitivity of the time step without showing any result.
Author's answer: We removed this paragraph from the manuscript. However, this issue is discussed in more detail by answering the second Referee Comment, what we gladly refer to.
Modification(p12 l 26-35): [..]Removed this section.

RC2(18):P13 l 4 : what is the reference to say that liquid water is overestimated ? Why do not you use the observed value?
Author's answer: There is no observed value for this fog event. Our assumptions that the value of the saturation adjustment is overestimated is based on theoretically consideration and on literature found information that conditions for applying saturation adjustment are violated here. However, since this is no evidence for an overestimation in comparison to the real value we replaced this phrase by "higher".
Modification(p13, l4): [..] higher in the case of saturation adjustment.

RC2(19): Fig 7 : n_c is a 3D field. So is it a vertical and horizontal average, or is it for the first vertical level?
Author's answer: It is a horizontal and vertical average for the whole fog layer. Corrected in the revised version.
Modification(Fig. 7): [..] (as a horizontal and vertical average of the fog layer) [..]

RC2(20):P 14 l 21 : as it is the explicit method, why do you take care of maximum supersaturation?

Author's answer: We revised this passage as we must admit that it was confusing to speak about maximum supersaturation for the explicit method, which is commonly used for activation parameterization in case of saturation adjustment. Our aim here was to show that we were able to reproduce typical observed values for the supersaturation. However, for that we do not need to refer to the maximum value. Mainly, those observed values are measured at a height of 2m. Accordingly, in the revised manuscript we connect the observed values with the shown values of simulation in 2m.
Modification(p?, l?): [..] while in case EXP and PRG average supersaturation of 0.05% in 2 m occur, which corresponds to typical within fog.

RC2(21): What is new from Fig. 9 and 10?
Author's answer: In Figure 9 and 10 the microphysical tendiencies are discussed in detail. In contrast to Fig. 5 they consider a full two-moment microphysics scheme, i.e. that also the droplet number concentration is altered. Due to that it could exemplary shown what processes and how strong certain processes influence the

RC2(22):p 16 : Could you conclude that the radiation impact of n_c is more important than in the sedimentation process ?
Author's answer: This is in interesting objection. Since, we focused here on the impact of microphysical parametrization (and the effect of the radiative impact of n_c is considered within the radiation model) we have not done studies yet to quantify the feedback to e.g. radiative cooling. To isolate this processes (since there is a feedback mechanism: radiative cooling produces higher supersaturation → leading to more activated droplets → leading to an decreased average radius (sine the surplus water vapor is distributed on more droplets) → slower sedimentation and → causes stronger radiative cooling, since the effective radius is decreased → leading to new (maybe stronger) supersaturation) more studies must be conducted to answer this question appropriately. Moreover, for the sedimentation process a similar feedback mechanism is involved. which might be shortly outlined as: if the number of droplets decrease due to sedimentation → the water vapor surplus is distributed on less droplets → leading to higher average radius → lesser optical thickness and → stronger sedimentation.
To get an quantitative idea which of those processes is more important determining the life cycle of the fog would include two more simulation in which the number concentration is kept constant on the one hand for the radiation effect and on the other hand for the sedimentation process.
Modification: None.

RC2(23): Fig 9 : it would be better to put the total tendency in b than in c, as profiles are too intermingled in c.
Author's answer: We agreed and modified the figures as we put the total tendency in an own plot.
Modification(Fig. 9 & 10) [..] Modified Fig. 9 and Fig. 10.

RC2(24): Fig 10 : Deactivation means evaporation?
Author's answer: Yes, it does. Due to reasons of consistency it is adapted to equation 2.
Modification(FIG10): [..] deactivation → evaporation

Misspelling :
- p1 l 20 : aerosols
- p2 l 9 : as as
- p12 l 21 : diminishes
- p14 l 18 : is→ are

- p 15 l 16 : shows

All misspellings are corrected in the revised version.

Large-eddy simulation of radiation fog with comprehensive two-moment bulk microphysics: Impact of different aerosol activation and condensation parameterizations

Johannes Schwenkel[1] and Björn Maronga[1,2]

[1]Institute of Meteorology and Climatology, Leibniz Universität Hannover, Hannover, Germany
[2]Geophysical Institute, University of Bergen, Bergen, Norway

Correspondence to: Johannes Schwenkel (schwenkel@muk.uni-hannover.de)

Abstract. In this paper we study the influence of the cloud microphysical parameterization~~on large-eddy simulations .~~, namely the effect of different treatment of diffusional growth and aerosol activation, on the structure and life cylce of radiation fog ~~.~~ ~~A~~ in large-eddy simulations. For this purpose we investigate a selected deep fog case as observed at Cabauw (Netherlands) ~~is investigated~~ using high-resolution large-eddy simulations with ~~different microphysics treatments for activation and diffusional growth. A comparison of the results indicates that the commonly applied assumption of saturation adjustment produces at maximum 6.9% higher liquid water paths compared to the explicit diffusional growth method but has no significant influence on the general life cycle of the fog layer. Differences are found to be the most pronounced at the top of~~ comprehensive bulk cloud microphysics scheme. By comparing saturation adjustment with an explicit and a prognostic method for calculating supersaturation (while neglecting the activation process) we find that, even though assumptions for saturation adjustment are violated, the expected overestimation of the liquid water mixing ratio is negligible. By additionally considering activation, however, our results indicate that saturation adjustment, due to approximating the underlying supersaturation, leads to a higher droplet concentration and hence significantly higher liquid water content in the fog layer~~where the highest supersaturations occurs.~~ , while explicit and prognostic methods yield comparable results. Furthermore, the effect of different droplet number concentrations is investigated~~by using a selection of~~ , induced by using different common activation schemes. We find, in line with previous studies, a positive feedback between the droplet number concentration and ~~both the optical thickness and the~~ strength of the fog layer (defined by its vertical extent and amount of liquid water). Furthermore, we perform an explicit analysis of the budgets of condensation, evaporation, sedimentation and advection in order to assess which processes have the largest spatial ~~and temporal~~ influence on the development of the fog layer ~~.~~in its different development phases.

1 Introduction

The prediction of fog is an important part of the estimation of hazards and efficiency in traffic and economy (Bergot, 2013). The annual damage caused by fog events is estimated to be the same as the amount caused by winter storms (Gultepe et al., 2009). Despite improvements in numerical weather prediction (NWP) models, the quality of fog forecasts is still unsatisfactory. The explanation for this is obvious: fog is a meteorological phenomenon influenced by a multitude of complex physical processes.

Namely, these processes are radiation, turbulence, atmosphere-surface interactions, and cloud microphysics (hereafter referred to as microphysics), and which interact on different scales (e.g. Gultepe et al., 2007; Haeffelin et al., 2010). The key issue for improving fog prediction in NWP models is to ~~either resolve all relevant processes , or~~ resolve the relevant processes explicitly, or - if that is not possible - to parameterize them ~~appropriately~~in an appropriate way.

In recent years various studies have focused on the influence of microphysics on fog. In particular, the activation of ~~aersols~~aerosols (hereafter simply referred to as activation), which determines how many aerosols at a certain supersaturation get activated and hence can grow into cloud drops, is ~~of major~~ a key process and thus of special interest (e.g. Bott, 1991; Hammer et al., 2014; Boutle et al., 2018).

Stolaki et al. (2015) investigated and compared the influence of aerosols on the life cycle of a radiation fog event while using ~~two-dimensional large-eddy simulations (LESs)~~ the one-dimensional mode of the MESO-NH model with a two-moment warm microphysics scheme after Geoffroy et al. (2008) and Khairoutdinov and Kogan (2000) and included an activation parameterization after Cohard et al. (1998). In other fog studies, using single-column models, different activation schemes such as the simple Twomey-power law activation in Bott and Trautmann (2002) and the scheme of Abdul-Razzak and Ghan (2000) (see Zhang et al., 2014) were applied. Furthermore, also more advanced methods such as sectional models have been used for an appropriate activation representation. Maalick et al. (2016) used the ~~SALSA module~~ Sectional Aerosol module for Large Scale Applications (SALSA) (Kokkola et al., 2008) in two-dimensional studies for a size-resolved activation. Mazoyer et al. (2017) conducted similar to Stolaki et al. (2015) simulation of the ParisFog with the MESO-NH model but using the 3D-Large-Eddy Simulation (LES) mode, and focusing on the influence of drag effect on droplet deposition. For the fog microphysics they also used an activation parameterizations after Cohard et al. (2000) in connection with saturation adjustment. This large number of different activation parameterizations raises the question ~~of the quantitative differences between the individual methods~~ how different methods affect the structure and life cycle of radiation fog. Furthermore, schemes that parameterize activation based on updrafts might fail for fog. Such schemes derive supersaturation as ~~as~~ a function of vertical velocity, which is valid for ~~common clouds~~ convective clouds that are forced by surface heating, but not for radiation fog, which is mainly driven by longwave radiative cooling ~~(Boutle et al., 2018).~~

in its mature phase (Maronga and Bosveld, 2017; Boutle et al., 2018).

Although great progress has been made to understand different microphysical processes in radiation fog based on numerical experiments, turbulence as a key process has been either fully parameterized (single-column models) or oversimplified (two-dimensional LES). Since turbulence is a fundamentally three-dimensional process, the full complexity of all relevant mechanisms can only be reproduced with three-dimensional LESs (Nakanishi, 2000).

Moreover, a disadvantage of ~~the~~ most former studies is the use of saturation adjustment, which implies that supersaturations are immediately removed within one time step. This approach is only valid when the time scale for diffusion of water vapour (on order of 2-5 s) is much smaller than the model time step, which is the case in large scale models where time steps are on the order of 1 min. However, in LES ~~(as in the present study), the time step easily goes~~ of radiation fog, time steps easily go down to split seconds so that this assumption is violated and might lead to excessive condensation (e.g. Lebo et al., 2012).

~~This paper addresses two issues related to the microphysics parameterization in numerical models to simulate radiation fog. Firstly, the error introduced by using saturation adjustment for simulating fogin LES models will be analyzed and compared with an explicit approach for diffusional growth. Secondly, the influence of different numbers of activated aerosol by using different Twomey-based activation schemes on the simulated fog layer is investigated with the focus on feedback effects with the fog microphysics~~ Following Lebo et al. (2012) and Thouron et al. (2012), who investigated the influence of different supersaturation calculations for deep convective cloud and stratocumulus, the present work considers the effect of saturation adjustment on radiation fog.

As Mazoyer et al. (2017) and Boutle et al. (2018) stated that both, LES and NWP models tend to overestimate the liquid water content and the droplet number concentration for radiation fog the following questions are derived from these shortcomings:

(i) Is saturation adjustment appropriate as it crucially violates the assumption of equilibrium? How large is the effect of different supersaturation calculations on diffusional growth?

(ii) What is the impact of different activation schemes on the fog life cycle for a given aerosol environment?

(iii) As the number of activated droplets is essentially determined by the supersaturation, how large is the effect of different supersaturation modeling approaches on aerosol activation and therewith on the strength and life cycle of radiation fog (cf. Thouron et al., 2012)?

In the present paper we will address the above issues by employing high-resolution LESs based on an observed typical deep fog event with continental aerosol conditions.

The paper is organized as follows: Section 2 outlines the methods used, that is the LES modeling framework and the microphysics parameterizations used. Section 3 provide an overview of the simulated cases and model setup, while results are presented in section 4. Conclusions are given in section 5.

2 Methods

This section will outline the used LES model and the treatment of radiation and land-surface interactions, followed by a more detailed description of the bulk microphysics implemented in the Parellized Large-Eddy Simulation Model (PALM) and the extensions made in the scope of the present study.

2.1 LES model with embedded radiation and land surface model

In this study the LES model PALM (Maronga et al. 2015; revision 2675 and 3622) was used with extensions in the microphysics parameterizations. PALM has been successfully applied to simulate the stable boundary layer (BL) (e.g. during the first intercomparison of LES for stable BL, GABLS, Beare et al., 2006) as well as radiation fog (Maronga and Bosveld, 2017). The model is based on the ~~non-hydrostatic~~ incompressible Boussinesq-approximated Navier-Stokes equations, and prognostic equations for total water mixing ratio, potential temperature, and subgrid-scale turbulence kinetic energy. PALM is discretized in space using finite differences on a Cartesian grid. For the non resolved eddies a 1.5-order flux-gradient subgrid closure scheme after Deardorff (1980) is applied, which includes the solution of an additional prognostic equation for the subgrid-scale TKE. Moreover, the discretization for space and time is done by a fifth-order advection scheme after Wicker and Skamarock (2002) and a third-order Runge-Kutta time-step scheme (Williamson, 1980), respectively. The interested reader is referred to Maronga et al. (2015) for a detailed description of the PALM model.

In order to account for radiative effects on fog and the Earth's surface energy balance, the radiation code RRTMG (Clough et al., 2005) has been recently coupled to PALM, running as an independent single column model for each vertical column of the LES domain. RRTMG calculates the radiative fluxes (shortwave and longwave) for each grid volume while considering profiles of pressure, temperature, humidity, liquid water and the droplet number concentration (n_c). Compared to the precursor study of Maronga and Bosveld (2017), improvements in the microphysics parameterization introduced in the scope of the present study allow a more realistic calculation of the fog's radiation budget, since n_c is now represented as a prognostic quantity instead of the previously fixed value. This favors an improved calculation of the effective radius, which is given as

$$r_\mathrm{eff} = \left(\frac{3\, q_\mathrm{l}\, \rho}{4\pi\ n_\mathrm{c} \rho_\mathrm{l}} \right)^{\frac{1}{3}} \exp(\log(\sigma_\mathrm{g})^2), \tag{1}$$

where q_l is the liquid water mixing ratio, ρ the air density, ρ_l being density of water and σ_g=1.3 the geometric standard deviation of the droplet distribution. The effective droplet radius is the main interface between the optical properties of the cloud and the radiation model RRTMG. Note, that 3D radiation effects of the cloud are not implemented in this approach, which however could affect the fog development at the lateral edges during formation and dissipation phases when no homogeneous fog layer is present. Radiation calculations traditionally require enormous ~~computation~~ computational time, the radiation code is called at fixed intervals on the order of 1 min only.

Moreover, PALM's land surface model (LSM) is used to calculate the surface fluxes of sensible and latent heat. The LSM consists of multi-layer soil model, predicting soil temperature and soil moisture, as well as a solver for the energy balance of the Earth's surface using a resistance parameterization. The implementation is based on the ECMWF-IFS land surface parametrization (H-TESSEL) and its adaptation in the DALES model (Heus et al., 2010). A description of the LSM and a validation of the model system for radiation fog is given in Maronga and Bosveld (2017).

2.2 Bulk microphysics

As a part of this study, the two-moment microphysics scheme of Seifert and Beheng (2001; 2006) implemented in PALM, which basically only predicts the rain droplet number concentration (n_r) and cloud water mixing (q_r) ~~is~~ was extended by prognostic equations for n_c and cloud water mixing ratio (q_c). The scheme of Seifert and Beheng (2001; 2006) is based on the separation of the cloud and rain droplet scale by using a radius threshold of 40 µm. This separation is mainly used for parameterizing coagulation processes by assuming different distribution functions for cloud and rain droplets. However, as collision and coalescence are weak in fog due to small average droplet radii, the production of rain droplets is negligible.

Consequently, only the number concentration and mixing ratio of droplets (containing all liquid water and thus abbreviated with q_l here) are considered in the following. The budgets of the cloud water mixing ratio and number concentration are given by

$$\frac{\partial q_\mathrm{l}}{\partial t} = -\frac{\partial u_i q_\mathrm{l}}{\partial x_i} + \left(\frac{\partial q_\mathrm{l}}{\partial t}\right)_\mathrm{activ} + \left(\frac{\partial q_\mathrm{l}}{\partial t}\right)_\mathrm{cond} - \left(\frac{\partial q_\mathrm{l}}{\partial t}\right)_\mathrm{auto} - \left(\frac{\partial q_\mathrm{l}}{\partial t}\right)_\mathrm{accr} - \left(\frac{\partial q_\mathrm{l}}{\partial t}\right)_\mathrm{sedi}, \tag{2}$$

$$\frac{\partial n_\mathrm{c}}{\partial t} = -\frac{\partial u_i n_\mathrm{c}}{\partial x_i} + \left(\frac{\partial n_\mathrm{c}}{\partial t}\right)_\mathrm{activ} - \left(\frac{\partial n_\mathrm{c}}{\partial t}\right)_\mathrm{evap} - \left(\frac{\partial n_\mathrm{c}}{\partial t}\right)_\mathrm{auto} - \left(\frac{\partial n_\mathrm{c}}{\partial t}\right)_\mathrm{accr} - \left(\frac{\partial n_\mathrm{c}}{\partial t}\right)_\mathrm{sedi}. \tag{3}$$

The terms on the right-hand side represent the decrease or increase by advection, activation, diffusional growth, autoconversion, accretion, and sedimentation (from left to right). Following Ackerman et al. (2009), cloud water sedimentation is parameterized assuming that droplets are having a log-normal distribution and following a Stokes regime. This results in a sedimentation flux of

$$F_{q_\mathrm{l}} = k\left(\frac{4}{3}\pi\rho_\mathrm{l} n_\mathrm{c}\right)^{-2/3} (\rho q_\mathrm{l})^{\frac{5}{3}} \exp(5\ln^2\sigma_\mathrm{g}), \tag{4}$$

with ~~ρ_l being density of water, the parameter $k = 1.2\times10^8$~~the parameter $k = 1.2\cdot10^8$ $\mathrm{m^{-1}s^{-1}}$ ~~, and σ_g=1.3 the geometric standard deviation of the droplet distribution~~ (Geoffroy et al., 2010). The main focus of this paper is to ~~investigate the influence~~ study the effect of different microphysical parameterizations of activation and condensation processes on microphysical and macroscopic properties of radiation fog. Those different activation and condensation parameterizations will be discussed in the following.

2.2.1 Activation

It is well known that the aerosol distribution and the activation process are of great importance to the life cycle of fog (e.g. Gultepe et al., 2007). The amount of activated aerosols determines the number concentration of droplets within the fog, which in turn has a significant influence on radiation through optical thickness as well as on sedimentation and consequently influences macroscopic properties of the fog, such as its vertical extension. For these reasons, a sophisticated treatment of the activation process is an essential prerequisite for the simulation of radiation fog. Several parameterizations for bulk microphysics models have been developed to provide a realistic activation model. In this work, three of these activation schemes ~~will be~~ were compared with each other in order to quantify their influence on the development of a radiation fog event. The schemes considered in this scope are the simple activation scheme of Twomey (1959) which was used, e.g., by Bott and Trautmann (2002) to simulate radiation fog, the scheme of Cohard et al. (1998) (used by e.g. Stolaki et al., 2015; Mazoyer et al., 2017) and the one by Khvorostyanov and Curry (2006). The latter two represent an empirical and analytically extension of Twomeys scheme, respectively. Consequently, these parameterizations are frequently termed Twomey-type parameterizations with the general type of

$$N_\mathrm{CCN}(s) = N_0 s^k, \tag{5}$$

where N_{CCN} are the number of activated cloud condensation nuclei (CCN), N_0 and k are parameters depending on the aerosol distribution, and s is the supersaturation. This equation can be solved using several approaches and mathematical complexity levels. In the following, these three schemes and their underlying equations are presented.

1. **Twomey (1959):** The simple power law expression (see Eq. 5) is well known and has been used for decades to estimate the number of activated aerosol for a given air mass in dependence of the supersaturation. A weakness of this approach is that the parameters N_0 and k are usually assumed to be constant and are not directly linked to the microphysical properties. Furthermore, this relationship creates an unbounded number of CCN at high supersaturations.

2. **Cohard et al. (1998):** extended Twomey's power law expression by using a more realistic four-parameter CCN activation spectrum as shaped by the physiochemical properties of the accumulation mode. Although an extension to the multi-modal representation of an aerosol spectrum would be possible, all relevant aerosols that are activated in typical supersaturations within clouds and especially fog are represented in the accumulation mode (Cohard et al., 1998; Stolaki et al., 2015). Following Cohard et al. (1998) and Cohard and Pinty (2000) the activated CCN number concentration is expressed by

   $$N_{\mathrm{CCN}}(s) = Cs^k \underline{\times} \cdot F\left(\mu, \frac{k}{2}, \frac{k}{2}+1; \beta s^2\right) \tag{6}$$

   while C is proportional to the total number concentration of CCN that is activated when supersaturation s tends to infinity. Parameters k, μ, and β are adjustable shape parameters associated with the characteristics of the aerosol size spectrum such as geometric mean radius and the geometric standard deviation as well as with chemical composition and solubility of the aerosols. Thus, in contrast to a simple Twomey approach, the influence of physiochemical properties of the aerosol spectrum are taken into account.

3. **Khvorostyanov and Curry (2006):** have found an analytical solution to express the activation spectrum using Koehler theory. Therein, it is assumed that the dry aerosol spectrum follows a log-normal size distribution of aerosol f_d:

   $$f_d = \frac{dN_{\mathrm{a}}}{dr_{\mathrm{d}}} = \frac{N_{\mathrm{t}}}{\sqrt{2\pi}\ln\sigma_{\mathrm{d}} r_{\mathrm{d}}} \exp\left[-\frac{\ln^2(r_{\mathrm{d}}/r_{\mathrm{d0}})}{2\ln^2\sigma_{\mathrm{d}}}\right]. \tag{7}$$

   Here, r_{d} is the dry aerosol radius, N_{t} the total number of aerosols, σ_d is the dispersion of the dry aerosol spectrum, and r_{d0} is the mean radius of the dry particles. The number of activated CCN as a function of supersaturation s is then given by

   $$N_{\mathrm{CCN}}(s) = \frac{N_{\mathrm{t}}}{2}[1-\mathrm{erf}(u)]; \qquad u = \frac{\ln(s_0/s)}{\sqrt{2}\ln\sigma_{\mathrm{s}}}, \tag{8}$$

   where erf is the Gaussian error function, and

   $$s_0 = r_{\mathrm{d0}}^{-(1+\beta)}\left(\frac{4A^3}{27b}\right)^{1/2}, \qquad \sigma_s = \sigma_{\mathrm{d}}^{1+\beta}. \tag{9}$$

   In this case, A is the Kelvin parameter and b and β depend on the chemical composition and physical properties of the soluble part of the dry aerosol.

Since prognostic equations ~~are~~ were neither considered for the aerosols nor their sources and sinks, a fixed aerosol background concentration ~~is~~ was prescribed by setting parameters N_0, C and N_t for the three activation schemes. The different nomenclature of the aerosol background concentration is based on the nomenclature used in the original literature.

The activation rate is then calculated as

$$\left(\frac{\partial n_\mathrm{c}}{\partial t}\right)_{activ} = \max\left(\frac{N_\mathrm{CCN} - n_\mathrm{c}}{\Delta t}, 0\right), \tag{10}$$

where n_c is the number of previously activated aerosols that are assumed to be equal to the number of pre-existing droplets and Δt is the length of the model time step. It should be noted that this method does not represent the reduction of CCN. However, this error can be neglected since processes as aerosol washout and dry deposition are of minor importance for radiation fog. For all activation schemes it is assumed that every activated CCN becomes a droplet with an initial radius of 1 µm. This results in a change of liquid water, which is considered by the condensation scheme and is described in the next section. Furthermore, we performed a sensitivity study with initial radii of 0.5 µm to 2 µm, which showed that the choice of the initial radius had no impact on the results (not shown). This is consistent with the findings of Khairoutdinov and Kogan (2000) and Morrison and Grabowski (2007).

2.2.2 Condensation

The representation of diffusional growth~~and evaporation~~, evaporation, and calculating the underlying supersaturation is one of the fundamental tasks of cloud physics. Three different methods have been evaluated and widely discussed in the scientific community. Namely these are the saturation adjustment scheme, the simple explicit scheme, where the supersaturation is derived by the prognostic fields of temperature and water vapor, and a prognostic calculation method of the supersaturation following (e.g. Clark, 1973; Morrison and Grabowski, 2007; Lebo et al., 2012). Basically, the supersaturation is given by $s = q_\mathrm{v}/q_\mathrm{s} - 1$, while the absolute supersaturation (or water vapor surplus) is defined as $\delta = q_\mathrm{v} - q_\mathrm{s}$, where q_v is the water vapor mixing ratio and q_s is the saturation mixing ratio. In the following, these three methods are reviewed briefly.

1. **Saturation adjustment:** In many microphysical models, a saturation adjustment scheme is applied. The basic idea of this scheme is that all supersaturation is removed within one model time step and supersaturations are thus neglected; and thus potentially leads to excessive condensation. Despite the many years of application of this scheme, its influence on microphysical processes is discussed controversially in the community (e.g. Morrison and Grabowski, 2008; Thouron et al., 2012; Lebo et al., 2012). Saturation adjustment might hence especially be a source of error in fog simulations where very small time steps are used due to small grid spacings as outlined earlier. ~~In the following, both the saturation adjustment scheme and the explicit supersaturation calculation are presented.~~

2. ~~**Saturation adjustment:**~~ Using the saturation adjustment scheme, q_l represents a diagnostic value calculated by means of

$$q_\mathrm{l} = \max(0, q - q_\mathrm{r} - q_\mathrm{s}), \tag{11}$$

where q is the total water mixing ratio~~, and q_s is the saturation mixing ratio~~. The saturation mixing ratio, which is a function of temperature, is approximated in a first step by

$$q_{\mathrm{s}}(T_{\mathrm{l}}) = \frac{R_{\mathrm{d}}}{R_{\mathrm{v}}} \frac{e_{\mathrm{s}}(T_{\mathrm{l}})}{p - e_{\mathrm{s}}(T_{\mathrm{l}})}, \tag{12}$$

where T_{l} is the liquid water temperature and p ~~the~~ is pressure. The individual gas constants for dry air and water vapor are denoted R_{d} and R_{v}, respectively. For the saturation vapor pressure e_{s} an empirical relationship of Bougeault (1981) is used. In a second step q_{s} is corrected using a first-order Taylor series expansion of q_{s}:

$$q_{\mathrm{s}}(T) = q_{\mathrm{s}}(T_{\mathrm{l}}) \frac{1 + \beta q}{1 + \beta q_{\mathrm{s}}(T_{\mathrm{l}})}, \tag{13}$$

with

$$\beta = \frac{L_{\mathrm{v}}}{R_{\mathrm{v}} c_{\mathrm{p}} T_{\mathrm{l}}^2}, \tag{14}$$

where c_{p} is the specific heat of dry air and L_{v} is the latent heat of vaporization. As aforementioned, in each model time step, all supersaturation is converted into liquid water or, in subsaturated regions, the liquid water is reduced until saturation. Therefore, for using the saturation adjustment scheme and a calculation of aerosol activation, the supersaturation must be estimated. For that, using the activation scheme of Cohard et al. (1998) the supersaturation is estimated following Thouron et al. (e.g. 2012); Mazoyer et al. (e.g. 2017); Zhang et al. (e.g. 2014) and directly translated into a droplet number concentration by

$$s^{k+2} \cdot F\left(\mu, k/2, k/2+1, -\beta s\right) = \frac{\left(\phi_1 w + \phi_3 \frac{dT}{dt}|_{\mathrm{rad}}\right)^{3/2}}{2kC\pi\rho_l\phi_2 B(k/2, 3/2)}, \tag{15}$$

where ϕ_1, ϕ_2 and ϕ_3 are functions of temperature and pressure and given in Cohard et al. (1998) and Zhang et al. (2014) . w is the vertical velocity and B the beta function.

3. **Explicit supersaturation calculation:** Supersaturation is calculated explicitly from ~~the predicted water vapor mixing ratio q_v and the~~ q_{v} and temperature T (from which q_{s} can be derived). However, since it is assumed that the supersaturation is kept constant during one model time step, the explicit approach requires a very small model time step of

$$\Delta t \leq 2\tau, \tag{16}$$

due to stability reasons (Árnason and Brown Jr, 1971). Here, τ is the supersaturation relaxation time which is approximated by

$$\tau \approx (4\pi D n_c \langle r \rangle)^{-1}, \tag{17}$$

where $\langle r \rangle$ is the average droplet radius, and D the diffusivity of water vapor in air. Due to the low dynamic time step in the present study imposed by the Courant-Friedrichs-Lewy criterion (on the order of 0.1 s), however, the condensation time criterion is fulfilled, and no additional reduction of the time step is needed. The rate of cloud water change due to condensation or evaporation is given by

$$\left(\frac{\partial q_\mathrm{l}}{\partial t}\right)_\mathrm{cond} = \frac{4\pi G(T,p)\rho_\mathrm{w}}{\rho_\mathrm{a}} s \int_0^\infty r f(r) dr \tag{18}$$

$$= \frac{4\pi G(T,p)\rho_\mathrm{w}}{\rho_\mathrm{a}} s r_\mathrm{c} \tag{19}$$

where r_c is the integral radius and $G = \frac{1}{F_\mathrm{K}+F_\mathrm{D}}$ included the thermal conduction and the diffusion of water vapor (Khairoutdinov and Kogan, 2000). The density ratio of liquid water and the solute is given by $\rho_\mathrm{w}/\rho_\mathrm{a}$. Using such a small time step allows the use of a diagnostic approach for the supersaturation calculation. ~~Nevertheless, pseudo-prognostic solutions are also used for the saturation calculation, which are able to mitigate~~

4. **Prognostic supersaturation:** The prognostic/ semi-analytic approach, which was first introduced by Clark (1973), includes an additional prognostic equation for the absolute supersaturation. Even though this requires further computational costs for solving one more prognostic equation, it mitigates the problem of spurious cloud-edge supersaturations ~~(Grabowski and Mor~~ ~~. Here, the error of these supersaturations , which tends to diminish with decreasing grid spacing and increasing advectionvelocity, can be considered to be small due to the relatively small grid spacing and relatively strong wind used in the present study (see next section).~~ and prevent inaccurate supersaturation caused by small errors in the advection of heat and moisture (Morrison and Grabowski, 2007; Thouron et al., 2012).

   The temporal change of the absolute supersaturation is given by

   $$\frac{\partial \delta}{\partial t} - \frac{1}{\rho}\nabla \cdot (u\, \rho\delta) = A - \frac{\delta}{\tau}, \tag{20}$$

   with A described by

   $$A = -q_\mathrm{s}\frac{\rho g w}{p - e_\mathrm{s}} - \frac{dq_\mathrm{s}}{dT}\cdot\left[\frac{gw}{c_\mathrm{p}} + \left(\frac{dT}{dt}\right)_\mathrm{rad}\right], \tag{21}$$

   with g being gravitational acceleration. The supersaturation relaxation time is given in Eq. 17. The second term on the left hand side of Eq. 20 describes the change of the absolute supersaturation due to advection, while the right hand side considers effects for δ to changes in pressure, adiabatic compression/expansion, and radiative effects (from left to right). By doing so, the predicted supersaturation is used for determining the number of activated droplets as well as the condensation and evaporation processes.

3 Case description and model setup

The simulations performed in the present study are based on an observed deep fog event during the night from 22 to 23 March 2011 at the Cabauw Experimental Site for Atmospheric Research (CESAR). The fog case is described in detail in

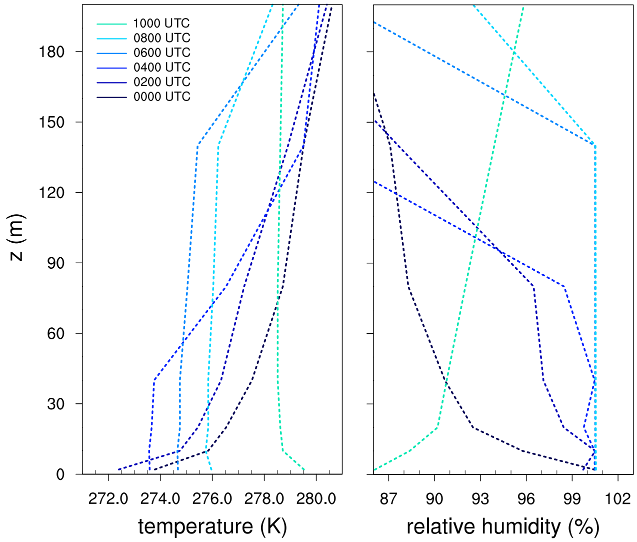

Figure 1. Profiles of potential temperature and relative humidity at different times as observed at Cabauw.

Boers et al. (2013) and was used as validation case for PALM in Maronga and Bosveld (2017). The CESAR site is dominated by rural grassland landscape and, although it is relatively close to the sea, there are typically continental aerosol conditions characterized by agricultural processes (Mensah et al., 2012).

The fog initially formed at midnight (as a thin near-surface layer), induced by radiative cooling, which also produced a strong inversion with a temperature gradient of 6 K between the surface and the 200 m tower-level. In the following the fog layer began to develop: At 0300 UTC the fog had a vertical extension of ~~below~~ less than 20 m~~increased to a fog top of 80-140~~, then deepened rapidly to 80 m, and reaching 140 m depth at 0600 UTC. At ~~this point~~0300 UTC, also the visibility ~~was reduced to~~ had reduced to less than 100 m. After sunset ~~which took place at~~ (around 0545 UTC~~a further development was suppressed , which led to an effective evaporation of the fog~~) a further invigoration close to the ground was suppressed and after 0800 UTC the fog starts quickly evaporate due to direct solar heating of the surface. For details, see Boers et al. (2013).

The model was initialized as described in the precursor study of Maronga and Bosveld (2017). Profiles of temperature and humidity (see Fig. 1) were derived from the CESAR 200 m-tower and used as initial profiles in PALM. A geostrophic wind of 5.5 m s^{-1} was prescribed based on the observed value at Cabauw at 0000 UTC.

The land surface model ~~is~~ was initialized with short grassland as surface type and four soil model layers at the depths of 0.07 m, 0.28 m, 1.0 m and 2.89 m. The measured surface layer temperatures ~~are~~ were interpolated to the respective levels, resulting in temperatures of 279.54, 279.60, 279.16, and 279.16 K for soil layers one to four, respectively. Furthermore, the initial soil moisture ~~is~~ was set to the value at field capacity (0.491 m^{3}m^{-3}), which reflects the very wet soil and low water table in the Cabauw area. The heat conductivity was set to $\Lambda = 4$, based on the radiation and energy balance observed at 0000 UTC at Cabauw. Moreover, the roughness length for momentum was prescribed to 0.15 m. Note that Maronga and Bosveld (2017) discussed that this value appears to be a little high given the season and wind direction. ~~For the purpose of the present study, this does , however not affect the purpose of~~ This does not play an important role for the present study~~.~~

~~The radiation model starts at 0000 UTC and uses a time step of 60 s, which is a good compromise between saving computational time and accuracy of the radiative fluxes and heating rates~~, however, as we will not focus on direct comparison against observational data from Cabauw.

All simulations start at 0000 UTC, before fog formation, and end at 1015 UTC on the next morning after the fog layer has fully dissipated. Precursor runs are conducted for additional 25 min using the initial state at 0000 UTC, but without radiation scheme and LSM in order to allow the development of turbulence in model without introducing ~~feedbacks~~ feedback during that time (see Maronga and Bosveld, 2017).

Based on sensitivity studies of Maronga and Bosveld (2017), a grid spacing of $\Delta = 1\,\text{m}$ ~~is~~ was adopted for all simulations, with a model domain size of 768 x 768 x 384 grid points in x-, y-, and z-direction, respectively. A sponge layer was used starting at a height of 344 m in order to prevent gravity waves ~~to be~~ from being reflected at the top boundary of the model.

Tab.1 gives on overview over the simulation cases. All cases ~~are~~ were initialized with (identical) continental aerosol conditions. Case ~~REF~~ SAT represents a reference run with no activation scheme and thus a prescribed constant value of $n_\text{c} = 150\,\text{cm}^{-3}$ (estimated from simulations of Boers et al. (2013)). This case represents a similar setup to the one described in Maronga and Bosveld (2017). Condensation processes ~~are~~ were here treated with the saturation adjustment scheme (Seifert et al., 2006). In order to evaluate the influence of saturation adjustment on the development of radiation fog, identical assumptions ~~are~~ were made in case ~~C1~~EXP and PRG, except that diffusion growth ~~is~~ was calculated with the explicit and prognostic method (see section 2.2.2)~~. Cases N1-N3 use~~ , respectively. Cases N1EXP-N3EXP used the activation schemes described in chapter 2.2.1. To ensure comparability between the different schemes, all of them ~~are~~ were initialized with a continental aerosol background described in Cohard et al. (1998), which is characterized by an aerosol with the chemical composition of ammonium sulfate [$(NH_4)_2SO_4$], a background aerosol concentration of $842\,\text{cm}^{-3}$, a mean dry aerosol radius of $r_\text{d0} = 0.0218\,\mu\text{m}$, and a dispersion parameter of the dry aerosol spectrum of $\sigma_\text{d} = 3.19$. For the Twomey activation scheme this results in $N_0 = 842\,\text{cm}^{-3}$ and $k = 0.8$ which is a typical value for the exponent for continental air masses ~~(e.g. Pruppacher and Klett, 1997, page 289 ff)~~ (e.g. Pruppacher and Klett, 1997, pages 289 et seq.). The Twomey activation scheme does not allow for taking aerosol properties into account. In contrast, the activation scheme of Cohard et al. (1998) requires the parameters C, k, β and μ to be derived from the aerosol properties. Here, values of $C = 2.1986 \cdot 10^6\,\text{cm}^{-3}$, $k = 3.251$, $\beta = 621.689$ and $\mu = 2.589$ ~~are~~ were used as described in Cohard and Pinty (2000). Finally, the activation scheme of Khvorostyanov and Curry (2006) can directly consider the aerosol properties, which are prescribed as aforementioned. Since changing other microphysical properties (such as mean geometric radius, chemical composition, or dispersion of dry aerosol spectrum) will have a similar effect to the physical outcomes as the variation of the aerosol concentration (because only cloud number concentration is affected), further simulation cases ~~are omitted.~~ were omitted. Moreover, for investigating the impact of the supersaturation calculation on CCN activation (see section 4.4) the simulation N2SAT, N2EXP and N2PRG were compared to each other. In all three cases the activation scheme of Cohard et al. (1998) is used.

Table 1. Overview of conducted simulations. The droplet number concentration n_c is only ~~given~~ prescribed for simulations without activation scheme. In the simulations ~~N1–N3~~ N1EXP-N3EXP n_c is a prognostic quantity and thus variable in time and space. The aerosol background concentration is abbreviated with $\mathrm{N}_{\mathrm{a,tot}}$, and used to initialize the activation schemes. Note for the scheme of (Cohard et al., 1998) a conversion to the parameter C must be applied, while for both other activation schemes this value is directly used to prescribe N_0 and N_t, respectively.

#	Simulation	Activation scheme	n_c [cm^{-3}]	$\mathrm{N}_{\mathrm{a,tot}}$ [cm^{-3}]	Condensation scheme
1	~~REF~~ SAT	none	150	none	~~saturation-adjustment~~ saturation adjustment
2	~~C1~~ EXP	none	150	none	explicit
3	~~N1~~ PRG	none	150	none	prognostic
4	N1EXP	Twomey (1959)	not fixed	842	explicit
~~4~~ 5	~~N2~~ N2EXP	Cohard et al. (1998)	not fixed	842	explicit
~~5~~ 6	~~N3~~ N3EXP	Khvorostyanov and Curry (2006)	not fixed	842	explicit
7	N2SAT	Cohard et al. (1998)	not fixed	842	saturation adjustment
8	N2PRG	Cohard et al. (1998)	not fixed	842	prognostic

4 Results

4.1 General fog life cycle and macrostructure

The reference case ~~REF~~ SAT is conducted with a constant droplet number concentration of $n_\mathrm{c} = 150\,\mathrm{cm}^{-3}$. The deepening of the fog layer can be seen in Fig. 2, which shows the profiles of the potential temperature, relative humidity and liquid water mixing ratio at different times.

The fog onset is at 0055 UTC, defined by a visibility below 1000 m and a relative humidity of 100%. In the following the fog layer deepens and extends to a top of approximately 20 m at 0200 UTC. However, at this point the stratification of the layer is still stable with a temperature gradient of 6 K between the surface and the fog top. The persistent radiative cooling of the surface and the fog layer leads to a further vertical development of the fog, which is accompanied with a regime transition from stable to convective conditions within the fog layer (see Fig. 2a). This starts as soon as the fog layer begins to become optically thick (at 0330 UTC), and when radiative cooling at the fog top becomes the dominant process, creating a top-down convective boundary layer. The highest liquid water mixing ratio of $q_\mathrm{l} = 0.41\,\mathrm{g\,kg}^{-1}$ is achieved at 0600 UTC at a height of 60 m (see Fig. 2c), while the the fog layer in total reaches the maximum one hour later at 0700 UTC. The lifting of the fog, which is defined by a non-cloudy near-surface layer ($q_\mathrm{l} \leq 0.01\,\mathrm{g\,kg}^{-1}$), occurs at 0845 UTC. At 1130 UTC the fog is completely dissipated.

4.2 ~~Saturation adjustment vs. explicit condensation~~Influence of different supersaturation parameterizations on diffusional growth

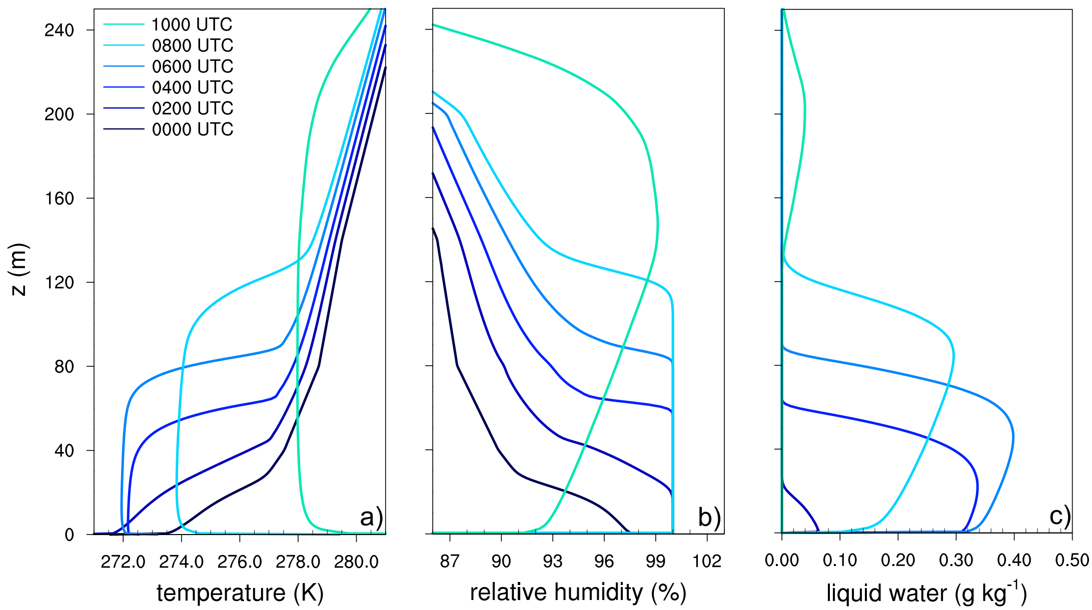

Figure 2. Profiles of potential temperature (a), relative humidity (b) and liquid water mixing ratio (c) at different times for the reference case REF.

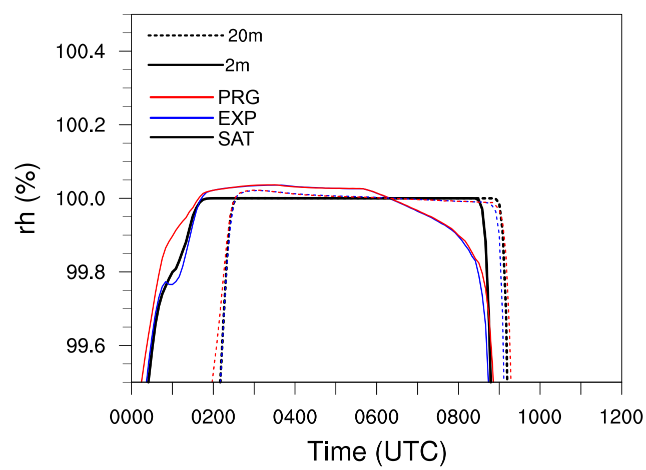

Figure 3. Time series of ~~height averaged~~ horizontal-averaged relative humidity/supersaturation at height levels of 2 m (dotted) and 20 m (dashed) ~~as well as the domain wide maximum (solid)~~ for ~~cases REF and C1~~different methods in treating the supersaturation calculation.

~~Absolute difference of liquid water mixing ratio from the C1 minus REF. Time marks of formation, maximum liquid water content, lifting, and dissipation are marked by plus signs, circles, crosses, and squares, respectively.~~

In this section we discuss the error introduced ~~when using a saturation adjustment scheme for the simulation of~~ by using saturation adjustment for simulating radiation fog. For this, we compare ~~two simulations with almost~~ three simulations with identical setup (cases ~~Ref and C1). Activation~~ SAT, EXP, and PRG), differs only in the way how supersaturation is calculated and consequently the amount of condensed or evaporated liquid water. To isolate this effect, activation is neglected in ~~both cases and the~~ all cases and n_c is set to a constant value of $150\,\mathrm{cm}^{-3}$. The effect on different supersaturations driving the diabatic process of activation is discussed in section 4.4. Due to the small grid spacing of 1 m used in our simulations, the time ~~steps are on~~ step is in the order of 10^{-1} s, which is more than one order of magnitude smaller than the allowed values of 2-5 s for assuming saturation adjustment (Thouron et al., 2012). The present case hence is an ideal environment evaluating the error introduced by using saturation adjustment and by keeping all other parameters ~~the same~~fixed.

Figure 3 shows time series of the horizontally-averaged saturation (supersaturation) for ~~REF and C1~~ SAT, EXP and PRG case. In ~~both~~ all cases saturation occurs simultaneously around ~~0100~~0120 UTC. In case ~~REF~~SAT, relative humidity does not exceed 100% due to its limitation by saturation adjustment, while in case ~~C1 maximum supersaturations of 0.12%~~ EXP and PRG average supersaturations of 0.05% in 2 m occur, which corresponds to typical values within fog ~~. For example, in the simulations of both Mazoyer et al. (2017) and Boutle et al. (2018) values close to 0.1% were observed, and in-situ observations during the ParisFog experiment revealed supersaturations of 0.05% (Hammer et al., 2014)~~(Hammer et al., 2014; Mazoyer et al., 2017; Boutle et al., 20
.

~~Case C1 also shows that the supersaturation reaches its maximum at 0345 UTC and persists until 0700~~For case EXP and PRG starting from 0615 UTC ~~. At~~ (in 2 m ~~and~~ height) and 0715 UTC (in 20 m height~~, however, supersaturation is in the range of 0.05%. Starting from 0350 UTC and 0315 UTC, respectively~~), supersaturations are removed and the air becomes subsaturated (on average). This is in contrast with case ~~REF~~ SAT, where the saturation adjustment approach keeps the relative humidity at 100% as long as liquid water is present (i.e. until the fog has dissipated). Around 0600 UTC, which is shortly after sunrise, relative humidity drops rapidly as a direct consequence of ~~solar radiation heating~~ direct solar heating of the surface and the near-surface air, preventing further supersaturation at these heights. While we cannot clearly identify the lifting of the fog in case ~~C1~~ EXP and PRG (due to the limited humidity range displayed), we note that for case ~~REF~~ SAT we can identify lifting times as a decrease of relative humidity around 0845 UTC at 2 m height and around 0910 UTC at 20 m height.

Beside this inherent difference in relative humidity, the general time marks (formation, lifting, dissipation, defined as in Maronga and Bosveld (2017)) of the fog layer are ~~very similar for cases REF and C1.~~ identical for cases SAT, EXP and PRG. ~~This allows a direct comparison of both cases.~~

~~In Fig. **??** the total difference of the liquid water mixing ratio q_l (REF minus C1) is shown. A clear tendency can be seen in the liquid water difference: On the top of the fog, where the highest supersaturation occurs due to radiative cooling, the largest differences in q_l of up to $0.06\,\mathrm{g\,kg^{-1}}$ can be observed (negative difference, blue). In general, the REF case shows higher values for q_l during the formation and mature phase of the fog. Close to the bottom where the net condensation is low (between 0400 UTC and 0600 UTC), the differences for q_l diminishes. Only in a few upper levels during lifting at a height of 240 m the C1 case exhibits higher liquid water mixing ratios.~~

~~This finding is directly linked to the used condensation schemes. The saturation adjustment scheme (REF) converts all excess moisture into liquid water. As long as diffusional growth (calculated via saturation adjustment) has a positive tendency, q_l will thus have higher values compared to case C1.~~

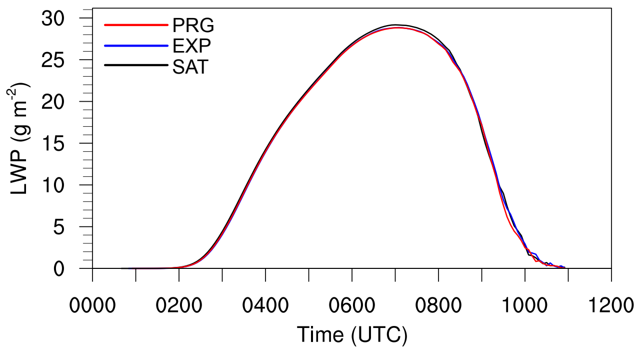

Figure 4. ~~Liquid~~ Time series of liquid water path (LWP) ~~of reference case REF~~ for cases using ~~the~~ saturation adjustment~~scheme and C1 case using an~~, the explicit ~~calculation of~~ approach and a prognostic method for the diffusional growth.

Figure 4 shows the liquid water path (LWP) for ~~both~~ all cases. Differences in the LWP appear between 0400 UTC and 1100 UTC and ~~are up to 6.9~~do not exceed 1% (lower values for ~~case C1). Simulations with a coarser grid spacing of 4 m (not shown), which result in a larger time step (approximately 0.6 s) for the same setup, exhibit nearly no differences for the different condensation schemes. As mentioned earlier and in previous publications the use of saturation adjustment is always a question of the time scales to be considered. This suggests that the effect of saturation adjustment on the integrated water content is negligible for simulations with sufficiently long time steps, but will lead to greater errors with decreasing time step. However, it can be summarized that , although the assumptions of saturation adjustment have no validity for the simulation of fog when using a very small time step, and the mean liquid water content is changed by nearly 7%, the general fog structure remains unaffected. We suppose that this finding is due to the very small supersaturation, which is not strong enough to generate a significant change in the effective radius which could lead to stronger sedimentation or an overall increased optical depth.~~ cases EXP and PRG), indicating that the choice of the condensation scheme does not affect the total water content of the simulated fog layer.

4.2.1 Budget of liquid water

Fig. 5 shows profiles for the liquid water mixing ratio (~~a~~left) as well as the liquid water budgets ~~(b-d)~~ at 0400 UTC, 0600 UTC and 0800 UTC for cases ~~REF and C1~~SAT, EXP and PRG. These times represent different stages of the fog development: deepening, mature phase, and mature phase development after sunrise, respectively. Figure 5a confirms that especially at the top of the fog, when it becomes ~~radiatively~~ radiative active, the liquid water is ~~overestimated~~ slightly higher in the case of saturation adjustment, but in general the differences between the runs are negligible. Figures 5 ~~b-d~~ (right) show a clear trend: On the one hand the sedimentation and advection rates are almost identical for ~~both~~ all cases at all times. On the other hand, clear differences can be observed in the production rate for condensation and the dissipation rate due to evaporation. In the case of saturation adjustment, these rates are almost twice as high (in absolute sense) as for the ~~C1 case~~ cases EXP and PRG over the entire height of the fog layer. This finding can be attributed to the fact that saturation adjustment is assuming the highest

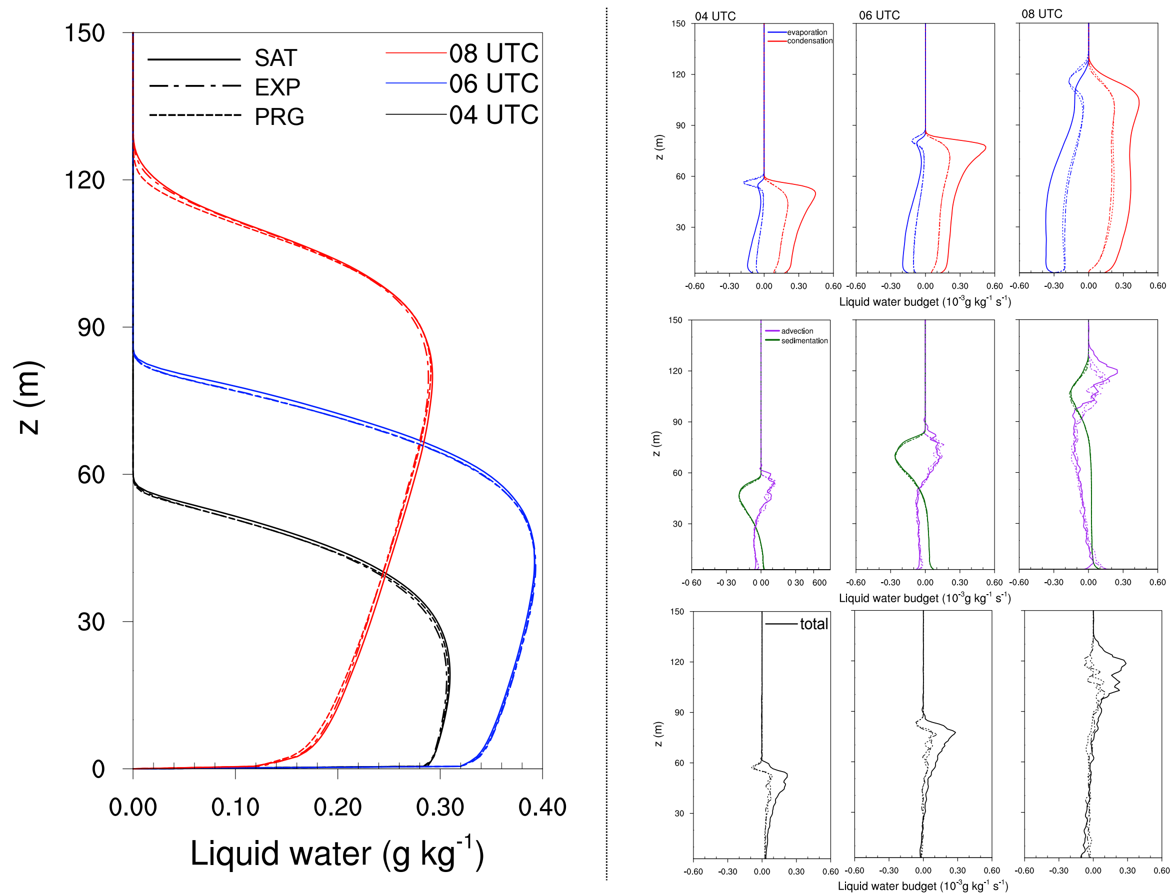

Figure 5. Instantaneous horizontally averaged profiles for the liquid water mixing ratio (~~a~~left) for 0400 UTC, 0600 UTC and 0800 UTC and budgets for q_l tendencies (~~b-d~~right, upper row: condensation and evaporation, middle row: sedimentation and advection and lower row: total tendency) for 0400 UTC, 0600 UTC and 0800 UTC for the simulations ~~REF~~ SAT, EXP and ~~C1~~PRG.

possible values for condensation. This in turn also affects the evaporation rates, which are counteracting the production by excessive condensation. The net effect, however, is ~~comparatively small . Interestingly, it can be observed thatthe condensation rates are significantly higher towards the top of the~~ small (c.f. Fig. 4).

It can be summarized that, although the assumptions of saturation adjustment are not valid for the simulation of fog when using ~~saturation adjustment. This agrees with the previous finding from Fig. **??** that more liquid water~~ a very small time step, the mean liquid water content is not changed by more than 1% and the general fog structure is not altered. This is probably due to the very small supersaturation that is ~~found in the upper part of the fog layer in case REF. This can be explained by the fact that the excessive condensation at the upper edge is caused by radiation cooling, which itself is proportional to the available liquid water content. This leads to a non-linear positive feedback mechanism, where the overestimation of condensation rates of the saturation adjustment scheme inherently produces too high values for q_l, which in turn is increasing radiative cooling~~

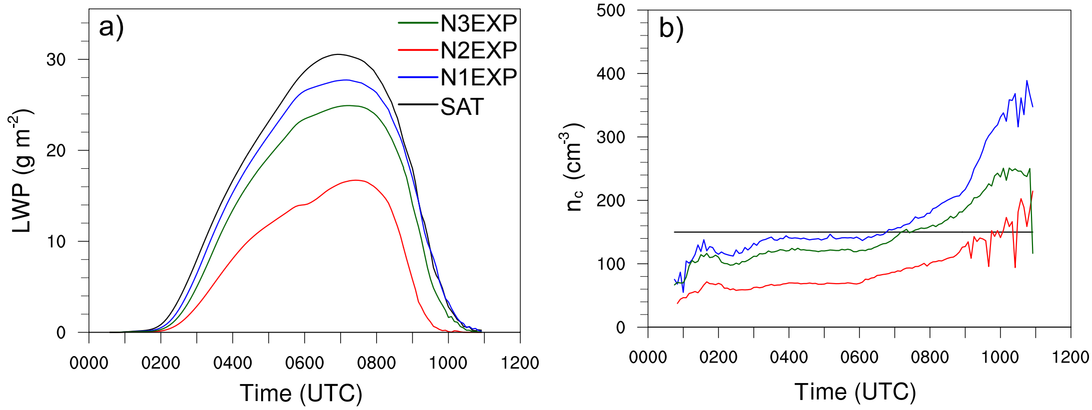

Figure 6. Time series of LWP and n_c (as a horizontal and vertical average of the fog layer) for the reference and ~~N1-N3~~ N1EXP-N3EXP case.

~~and hence producing new supersaturations which again are converted too fast into liquid water.~~ not strong enough to generate a significant change in the effective droplet radius, and which could lead to stronger sedimentation or higher radiative cooling rates. But as the different methods calculating supersaturation are not strong enough to create any noteworthy differences in condensational growth by using 1-moment microphysics (keeping the droplet number concentration constant), the impact of these differences for activation might be crucial and is discussed in section 4.4.

4.3 Comparison of different activation parameterizations

In numerous previous studies, the influence of aerosols and the activation process on the life cycle of fog was investigated (e.g. Bott, 1991; Stolaki et al., 2015; Maalick et al., 2016; Zhang et al., 2014; Boutle et al., 2018). Although all three activation schemes outlined in section 2.2.1 are comparable power law parameterizations that are initialized with identical aerosol spectra, the influence on ~~the~~ fog is still ~~to be investigated, since the~~ unknown, since changes in n_c ~~has a significant influence~~ due to different activation schemes have considerable effects on the life cycle of fog and thus also small differences ~~of the schemes can cause significant feedbacks~~in n_c might have a significant feedback.

Furthermore, n_c, as a function of time and averaged over the fog volume, is shown in Fig. 6b for the reference case and cases ~~N1-N3~~N1EXP-N3EXP, representing runs with the three different aerosol activation parameterization schemes (see Tab.1). The quantitative differences in the number of activated aerosol by using the different activation schemes is explained by a slightly different activation spectrum (see Appendix, Fig. A1). In principle, a similar qualitative development of n_c can be observed. While n_c increases during fog formation, it remains nearly constant during the mature phase of the fog~~for all cases~~. This can be explained by a constant longwave cooling at the fog top, producing ~~unvarying maximum supersaturations. However, as~~ similar supersaturations. As soon as the sun rises and the fog layers start to lift, all cases show a strong increase in ~~the~~ n_c. This increase can be explained by stronger supersaturations induced by thermal updrafts in the developing surface-driven convective boundary layer due to surface heating by solar radiation. Moreover, we note that while the qualitative course of

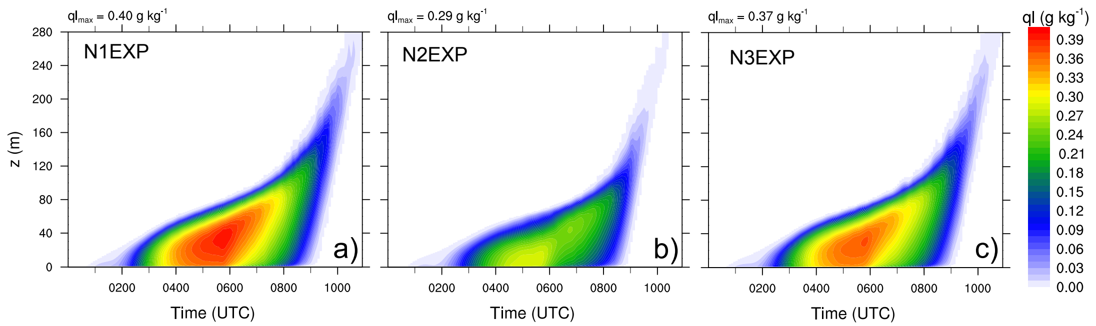

Figure 7. Height-time cross sections for the liquid water mixing ratio for ~~N1-N3~~N1EXP-N3EXP.

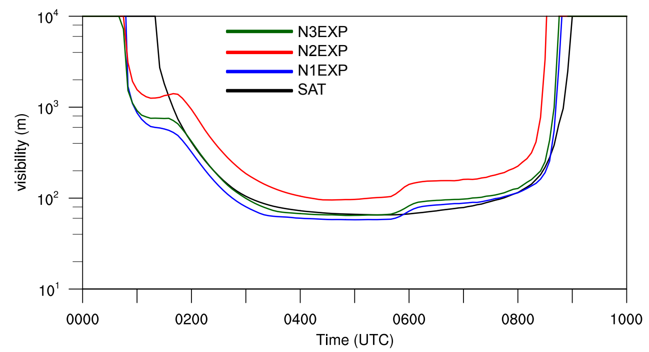

Figure 8. Time series of simulated visibility in 2 m height.

n_c is similar for all cases, the choice of the activation algorithm has an impact on number of activated ~~aerosol~~ aerosols and thus on the strength of the fog-layer (see Fig. 7). This is due to the radiation effect of the droplets. The number of droplets to which a certain amount of liquid water is distributed plays an important role: the larger the number of droplets, the larger is the radiation-effective surface and the higher also the optical thickness. As a result, on the one hand, the cooling rate from a fog with many small droplets is increased, allowing more water vapor to condense and the fog to grow stronger. On the other hand, however, sedimentation also depends on the droplet radius and plays a major role that will be discussed later. Time series of the LWP for the reference run and the three different cases are shown in Fig. 6a. The highest LWP occurs for the reference run which also shows the highest n_c during the formation and mature phase in comparison with the other simulations. Also for the cases ~~N1-N3~~ N1EXP-N3EXP a linear relationship between LWP and n_c can be found: A higher n_c leads to higher LWP. ~~On the one hand, this is due to the radiation effect of the droplets. The number of droplets to which a certain amount of liquid water is distributed plays an important role. The larger the number of droplets, the larger is the radiation-effective surface and thus also the optical thickness. As a result, the cooling rate from a fog with many small droplets is increased, allowing more water vapor to condense and the fog to grow more strongly. On the other hand, also sedimentation plays a major role which is discussed in~~

In Fig. 8 the simulated visibility for the cases N1EXP-N3EXP in 2 m height as well as the observed value is shown. Visibility is calculated from the LES data following following Gultepe et al. (2006) as

$$vis = \frac{1002}{(n_\mathrm{c}\,\rho\,q_\mathrm{l})^{0.6473}}, \tag{22}$$

(with n_c and q_l given in units of cm^{-3} and gm^{-3}, respectively). Hence, the visibility is significantly affected by the droplet number concentration and the liquid water content. In contrast to the former part of the study, where the droplet number concentration is a constant value, the analysis of the visibility is interesting here as the activation schemes significantly alter $\mathrm{n_c}$ and $\mathrm{q_l}$ for the different cases within the fog layer.

We note that visibility follows the same general temporal developed in all simulations with a rapid decrease during fog formation, deepening, and dissipation; with minimum values around 100 m (which is similar to the ~~following~~observations). We also see noteworthy differences, particularly shortly before 0200 UTC (before fog deepening) at around 0545 (shortly after sunrise). For both time marks, case N1EXP - N3EXP display sudden increases in visibility, due to an fast decrease of $\mathrm{n_c}$ in 2 m height; and which are not reproduced by case SAT, as $\mathrm{n_c}$ is fixed value in this case. Also, the time marks of formation and dissipation vary. For cases N1EXP - N3EXP the formation time is significantly advanced compared to case SAT, while dissipation time only shows a small tendency towards earlier times, at least for N1EXP and N3EXP. Case N2EXP displays a different behavior, with a later fog formation and higher visibility and accordingly earlier dissipation time. This is in line with the findings discussed above (i.e. a much weaker fog layer that, as a direct consequence, can dissipate much faster). Otherwise, all cases display almost identical visibility as soon as the fog has deepened.

4.3.1 Budgets of liquid water and droplet number concentration

Figure 9a shows the profiles of the liquid water mixing ratio at 0400 UTC, 0600 UTC, and 0800 UTC. ~~Here, it can be seen that the cases with higher values of q_l, integrated over the entire height, also contain most liquid water throughout the fog layer.~~ The maximum q_l in the fog layer is reached at approximately 0600 UTC at a height of 60 m. Afterwards a further vertical growth of the fog can be observed, where no further increase in liquid water takes places as a result of larger vertical extent of the mixing layer and due to rising temperatures after sunrise (see Fig. 5a). Moreover, Fig. 9b,c ~~shows~~ show the liquid water budget during the mature phase of the fog at 0600 UTC, when the fog was fully developed. Almost all three cases ~~shows~~ show identical values for condensation rates (see Fig. 9b) in the lowest part of the fog layer, with values being in the same order as the evaporation rates, so that the net gain in this region appears to be ~~negligible~~small. However, the ~~N2~~ N2EXP case (with the lowest n_c) exhibits a generally lower absolute evaporation rate compared to both other cases, which ~~is explained by~~ can be attributed to the slightly higher mean values of the relative humidity (not shown) than in ~~N1 and N3~~N1EXP and N3EXP. In the upper part of the fog layer, higher values of the condensation rate are observed (especially for ~~N1 and N3~~N1EXP and N3EXP) with a concurrent decrease in evaporation rates, ~~displaying the~~ leading to differently strong deepening of the fog layer. At a height of approximately 80 m a maximum of the evaporation rates can be observed, representing the presence of subsaturated regions in this height and the top of the fog. Larger differences can be observed in the sedimentation rates: First and foremost the sedimentation is proportional to the liquid water mixing ratio (see also Eq. 4). However, the strength of sedimentation also

Table 2. Table of fog's life cycle time marks.

Simulation	Onset	Maximum	Lifting	Dissipation
N1EXP	0025 UTC	0510 UTC	0810 UTC	1005 UTC
N2EXP	0050 UTC	0425 UTC	0755 UTC	0910 UTC
N3EXP	0025 UTC	0515 UTC	0810 UTC	0950 UTC

depends on the mean radius of the droplets, which increases with decreasing number of activated drops. Here, a lower n_c for a given amount of liquid water leads to a higher mean radius, compared to a higher n_c where the same amount of water is distributed to more drops, decreasing the mean radius. Integrated over height all three cases exhibit approximately the same sedimentation rates. Therefore, case ~~N2~~ N2EXP suffers the most from the loss of liquid water due to sedimentation (in relative terms). Moreover, Fig. 9c shows that sedimentation partially counteracts the gains caused by condensation at the upper edge of the fog. All in all it can be summarized that all shown processes affect the net change of the liquid water mixing ratio. However, in the mature phase sedimentation plays a key role, showing the highest values for the individual tendencies. As a result liquid water is slowly and constantly removed from the fog layer. These findings are in good agreement with investigations by Bott (1991). The sum of all tendencies, which is shown in Fig. 9d, is the height-dependent change of the liquid water. Also here it can be seen that in the lower 50 m the net tendency is negative, while in higher levels we observe a positive tendency, so that the fog continues growing vertically, while the liquid water content within the fog layer decreases.

Figure 10a shows profiles of n_c at 0400 UTC, 0600 UTC and 0800 UTC. We ~~see~~ note that the profiles of the different cases differ quantitatively but not qualitatively. The stage of the fog can thus be identified in the profiles for all cases: At 0400 UTC highest supersaturations occur close to the ground due to cooling of the surface and near-surface air, leading to high activation rates and therefore high n_c near the surface. At 0600 UTC a well-mixed layer has developed that is driven by the radiative cooling from the ~~fog-top~~fog top. While the turbulent mixing leads to a vertical well-mixed n_c, we note the maximum at the top, where the radiative cooling induces immense aerosol activation. This is also displayed in the budget of the n_c (see Fig. 10b,c), where the instantaneous rates for 0600 UTC are shown. Here, we see clearly that aerosol activation at the top of the fog layer is the dominant process in the mature phase of the fog, while activation near the surface is relatively unimportant. Also, we see that both, advection and sedimentation are much less important than activation. Finally, we note that ~~deactivation, while being small , does occur~~ evaporation of droplets, though small in magnitude, occurs at the fog top, reflecting updrafts of foggy air penetrating the subsaturated air aloft where droplets then evaporate.

The effect of the different activation schemes on the time of the fog life cycle is summarized in Tab. 2. While N1EXP and N3EXP have similar time marks, N2EXP stands out and show an delayed onset by 25 min, while the maximum liquid water mixing ratio is reached 45 min earlier, than in the other cases. Also lifting and dissipation are affected and occurred 15 min and 40 min (with respect to simulation N3EXP) earlier. This is due to a lesser absolute liquid water mixing ratio which evaporates faster by the incoming solar radiation. Therefore, it can be concluded that the use of different activation schemes (if they change

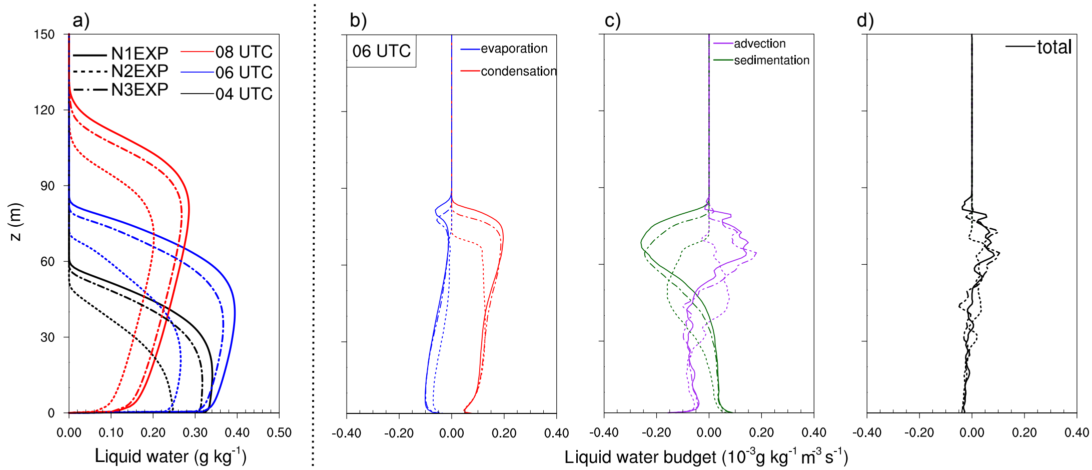

Figure 9. Profiles (instantaneously and horizontally averaged) of liquid water mixing ratio at 0400 UTC, 0600 UTC and 0800 UTC and profiles of explicit liquid water budget terms at 0600 UTC.

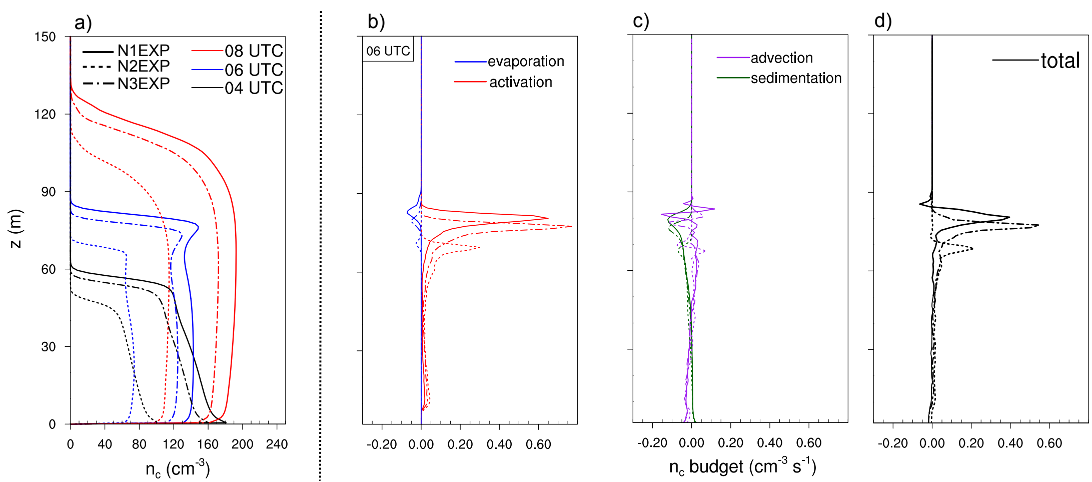

Figure 10. Profiles (instantaneously and horizontally averaged) of n_c at 0400 UTC, 0600 UTC and 0800 UTC and profiles of explicit n_c budget terms at 0600 UTC.

the droplet number concentration) has an effect on the time marks on the life cycle as well as on the fog height and the amount of liquid water within the fog layer.

4.4 Impact of supersaturation calculation on CCN activation

The impact of different methods modelling supersaturation on the CCN activation for a radiation fog event is investigated following Lebo et al. (e.g. 2012); Thouron et al. (e.g. 2012). Figure 11 shows the LWP for simulations applying the activation

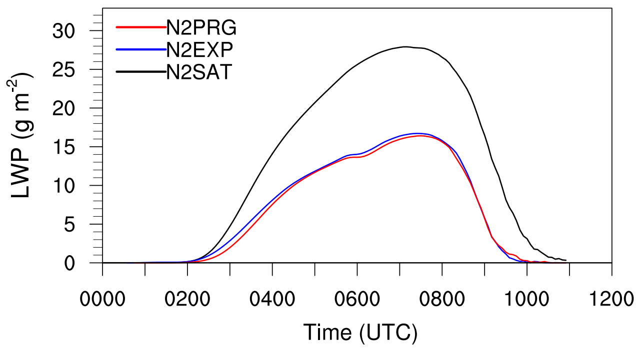

Figure 11. Time series of LWP for simulations using saturation adjustment (N2SAT, black), the explicit scheme (N2EXP, blue) and the prognostic method (N2PRG, red). All cases uses the activation scheme of Cohard et al. (1998).

scheme of Cohard et al. (1998) and using saturation adjustment (N2SAT), the explicit scheme (N2EXP) and a prognostic scheme (N2PRG) for calculating supersaturations. It can be seen that the prognostic approach and explicit methods produces very similar values for the LWP. However, in case of saturation adjustment the LWP is nearly 70% higher than for the other schemes. In Fig. 12 profiles of the liquid water mixing ratio (left) and droplet number concentration (right) are shown. Here, the number concentration in case N2EXP exhibits slightly higher values as N2PRG, but are both at approximately 100 $\mathrm{cm^{-3}}$ at 0600 UTC. In contrast, in simulation N2SAT a number concentration of 150 $\mathrm{cm^{-3}}$ is observed. Those differences are explained by the different methods for calculating the supersaturation, since activation is the main process altering the droplet number concentration (all other terms of Eq. 3 are less important as shown in Fig. 10). Due to that one can implicitly derive from the droplet number concentration that the prognosed and diagnosed values for the supersaturation using the explicit method and the prognostic method are quite similar. As saturation adjustment removes all supersaturation during one time step, a method for approximating the supersaturation is used (see Eq. 15). By that, the case N2SAT produces a droplet number concentration of 150 $\mathrm{cm^{-3}}$ at 0600 UTC, which is about 50% higher in comparision to N2EXP and N2PRG. However, these differences between N2SAT and N2EXP/N2PRG are in good agreement with the found values of Thouron et al. (2012) for a stratocumulus case (see their Fig. 2) where the number concentration of the explicit and prognostic method were also quite similar and the case with saturation adjustment overestimates the supersaturation and therefore the droplet number concentration. As outlined in the section before, the number concentration has a crucial impact on the LWP as well as on the times of lifting and dissipation of the fog.

4.4.1 Grid spacing sensitivity study

To evaluate the effect of grid spacing with different methods for calculating the supersaturation on CCN activation we repeated cases N2SAT, N2EXP and N2PRG each with two coarser grid spacings of 2 m and 4 m. The general effect of the grid spacing to the temporal development and structure of radiation fog is discussed in detail in Maronga and Bosveld (2017). In this section,

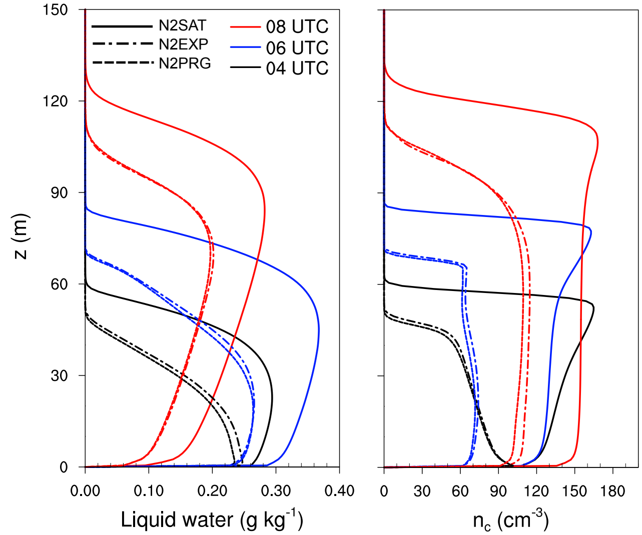

Figure 12. Profiles for liquid water mixing ratio and droplet number concentration at 0400 UTC, 0600 UTC and 0800 UTC.

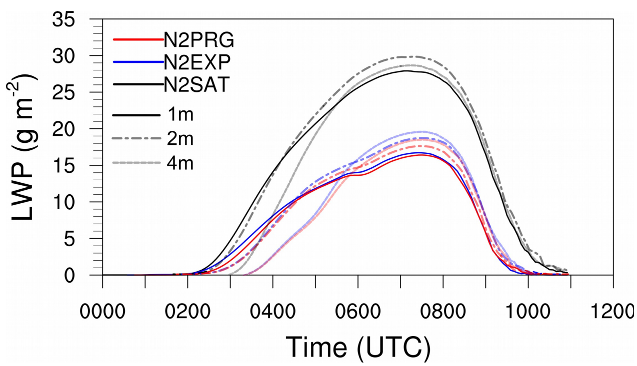

Figure 13. As Fig. 11 but also 2 m (dot-dashed) and 4 m (dashed).

we will thus focus only on relative changes in LWP due to different microphysical parameterizations at different spatial model resolution. In Fig.13 the LWP for the different supersaturation calculations and grid spacing is shown.

We note, that for all grid spacings the the major difference persists between the case using saturation adjustment, which produces a maximum value of approximately 30 g m^{-2} for the LWP in comparision to the explicit and prognostic method which both exhibit a maximum of approximately 20 g m^{-2}. However, interestingly, the relative differences (ratio of N2EXP to N2PRG) in the LWP between the explicit and prognostic methods increases as the grid spacing gets larger. Quantitatively speaking, in case of 1 m grid spacing the relative difference of the LWP is 2.1% between N2EXP and N2PRG during the mature phase while for the case with a grid spacing of 4 m it reaches 8.1%. This increase of the relative changes might be explained by the fact that the explicit scheme is very sensitive to small errors (e.g. induced by the numerical advection) in the fields of T and

q_v (e.g. Morrison and Grabowski, 2008; Thouron et al., 2012). A coarser spatial resolution favors that the error introduced by spurious supersaturation gets larger. Due to that we suppose that the increased differences (see Fig. 13) by larger grid spacings are induced by spurious supersaturation, which affect the CCN activation and by that infuence the LWP of the fog layer. As sedimentation and radiative cooling, which are key processes for fog, are sensitive to the number of activated droplets such errors should be considered.

5 Conclusions

The main objective of this work was to investigate the influence of the choice of the microphysical parameterization used in LES models on the life cycle of simulated nocturnal ~~radiation fog~~deep radiation fog under typical continental aerosol conditions. For this purpose we performed a series of LES runs for a ~~well-known~~ typical fog event observed at Cabauw (Netherlands). First, we compared the possible error introduced when using saturation adjustment in comparison with ~~the explicit representation of~~ an explicit and prognostic method for calculating the supersaturation for diffusional growth. The results showed that, although the model time step was inappropriate for the assumptions made during saturation adjustment, the differences in LWP are at most ~~6.9~~1% and the general life cycle ~~was~~ is not affected. This could be attributed to the fact that the typical supersaturations in fog are in the range of a few tenths of a percent, and the resulting absolute differences are too small to induce a further influence on dynamics, microphysics or radiation. ~~However, when looking in more detail, we found that the LES run with saturation adjustment produced higher liquid water mixing ratios in comparison to a comparative run using the explicit scheme for the whole fog layer with the largest differences at the fog top, caused by excessive condensation due to radiative cooling. These supersaturations are removed immediately by using the saturation adjustment scheme, leading to an overestimation of the liquid water mixing ratios, and due to a positive feedback mechanism to stronger radiative cooling and again to more liquid water content.~~

In a second part of our study, the effect of different activation schemes of Twomey (1959), Cohard et al. (1998) and Khvorostyanov and Curry (2006) on the simulated fog life cycle were investigated (cases ~~N1 to N3~~N1EXP to N3EXP). Even though these parameterizations are very similar, our results indicate that the resulting number of activated aerosols (and consequently the number of droplets)~~are~~, known to be a crucial parameter for the fog development~~and~~, differed significantly. An analysis of the budgets of n_c and q_l showed that diffusional growth is the major process for generating liquid water, but was found to be independent of the number of droplets and thus comparable in magnitude in all cases. In contrast, the sedimentation rates showed a different behaviour: On the one hand, these were found to be proportional to the liquid water mixing ratio, which is high in cases ~~N1 and N3~~N1EXP and N3EXP. On the other hand, the sedimentation depends on the mean radius of the droplets, which is higher in the case of fewer activated aerosols (case ~~N2~~N2EXP). Overall, this leads to almost identical absolute integral sedimentation rate for the three schemes. However, this means that liquid water is removed by sedimentation more rigorously in case N2 (in relative terms) compared to cases ~~N1 and N3~~N1EXP and N3EXP. Moreover, we could show that most aerosol activation happens near the surface during the formation phase of the fog, while the maximum number of activated aerosols during the mature phase is located at the top of the fog layer. The latter results from the radiative cooling of the fog top, producing the largest supersaturations. ~~However~~Nevertheless, this radiative cooling, triggers a top-down convective layer, so that the the droplets are well mixed, leading to an evenly distributed number concentration throughout the fog layer. As the sedimentation process and radiative cooling are proportional to the droplet number concentration, case N2EXP shows that the LWP is significantly reduced as a result of smaller droplet number concentrations. Moreover, the time marks of the fog life cycle are also affected: If the fog layer contains a smaller amount of liquid water, lifting and dissipation occur earlier, because less energy is required for evaporation of a thinner fog layer.

At last we investigated the impact of different (commonly used) supersaturation calculations on CCN activation by employing a single activation scheme but using the aforementioned different scheme considering supersaturation. From this study we found that in case of saturation adjustment higher droplet number concentration are produced. The explicit method and the prognostic method instead performed quite similar. However, in a grid spacing sensitivity study we observed that the relative differences between the prognostic and explicit approach increase as the spatial resolution decrease. We assume that this is due to larger errors of spurious supersaturations which lead to higher droplet concentrations and thus also effect the LWP.

In summary, the present study indicates that the choice of the used microphysics parameterization can be a key factor for the simulation of radiation fog. ~~At the moment, however~~While the effect of applying saturation adjustment in case of assuming a constant droplet number concentration on the diffusional growth is negligible, we recommend to use the prognostic approach to calculate the supersaturations in case of a full two-moment microphysics considering activation. Moreover, the choice of the chosen activation scheme has an noticeable impact of the LWP and fog height. However, we have no means to give advice ~~on which~~ which activation parameterization performs best.

In order to overcome these limitations of the present study, we plan to revisit this particular fog case using a Lagrangian particle-based approach to simulate the microphysics of droplets which will allow for explicitly simulating the development of the 3D droplet size distribution in the fog layer (e.g. Shima et al., 2009). This approach will also allow to resolve all relevant microphysical processes such as activation and diffusional growth instead of parameterizing them. As such simulations are computationally very expensive, only a very limited number of simulations are feasible at the moment, so that most future numerical investigations will - as in the present work - rely on bulk microphysics parameterizations. Based on the results using the Lagrangian approach, however, we hope to be able to give an educated recommendation on the best choice for such bulk parameterizations.

Code availability. The PALM model used in this study (revision 2675 and revision 3622) is publicly available on http://palm-model.org/trac/browser/palm?rev=2675 and http://palm-model.org/trac/browser/palm?rev=3622,respectively. For analysis, the model has been extended and additional analysis tools have been developed. The extended code, as well as the used Job-Setups and the used PALM source code are publicly available on https://doi.org/10.25835/0067929. All questions concerning the code-extension will be answered from the authors on request.

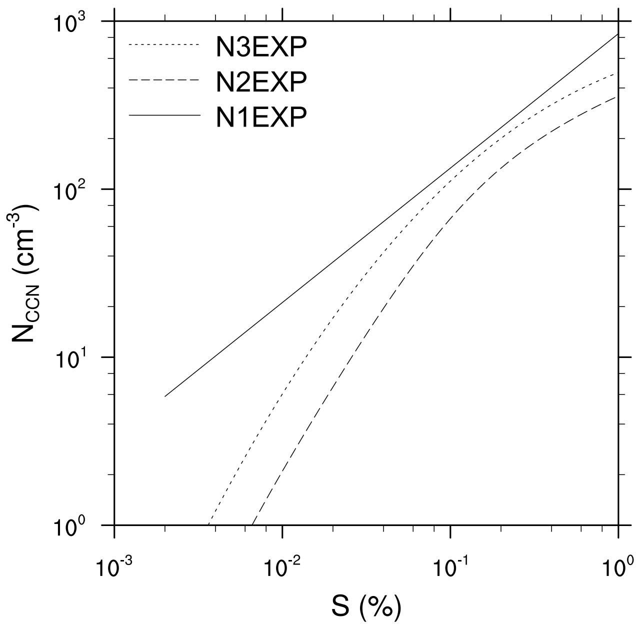

Figure A1. Activation spectrum for three different activation schemes of Twomey (1959)(~~N1~~N1EXP), Cohard et al. (1998)(~~N2~~N2EXP) and Khvorostyanov and Curry (2006)(~~N3~~N3EXP).

Appendix A: Activation spectrum

In Fig. A1 the activation spectrum for the three different activation schemes of Twomey (1959) (~~N1~~N1EXP), Cohard et al. (1998) (~~N2~~N2EXP) and Khvorostyanov and Curry (2006) (~~N3~~N3EXP) are shown.

Author contributions. The numerical experiments were jointly designed by the authors. JS implemented the microphysics parameterizations, conducted the simulations and performed the data analysis. Results were jointly discussed. JS prepared the manuscript, with significant contributions by BM.

Competing interests. The authors declare that they have no conflict of interest.

Acknowledgements. This work has been funded by the German Research Foundation (DFG) under Grant MA 6383/1-1, which is greatly acknowledged. All simulations have been carried out on the Cray XC-40 systems of the North-German Supercomputing Alliance (HLRN, https://www.hlrn.de/).

References

Abdul-Razzak, H. and Ghan, S. J.: A parameterization of aerosol activation: 2. Multiple aerosol types, J. Geophys. Res. Atmos., 105, 6837–6844, 2000.

Ackerman, A. S., VanZanten, M. C., Stevens, B., Savic-Jovcic, V., Bretherton, C. S., Chlond, A., Golaz, J.-C., Jiang, H., Khairoutdinov, M., Krueger, S. K., et al.: Large-eddy simulations of a drizzling, stratocumulus-topped marine boundary layer, Mon. Weather Rev., 137, 1083–1110, 2009.

Árnason, G. and Brown Jr, P. S.: Growth of cloud droplets by condensation: A problem in computational stability, J. Atmos. Sci., 28, 72–77, 1971.

Beare, R. J., Macvean, M. K., Holtslag, A. A., Cuxart, J., Esau, I., Golaz, J.-C., Jimenez, M. A., Khairoutdinov, M., Kosovic, B., Lewellen, D., et al.: An intercomparison of large-eddy simulations of the stable boundary layer, Boundary-Layer Meteorol., 118, 247–272, 2006.

Bergot, T.: Small-scale structure of radiation fog: a large-eddy simulation study, Quart. J. Roy. Meteor. Soc., 139, 1099–1112, 2013.

Boers, R., Baltink, H. K., Hemink, H., Bosveld, F., and Moerman, M.: Ground-based observations and modeling of the visibility and radar reflectivity in a radiation fog layer, J. Atmos. Ocean Technol., 30, 288–300, 2013.

Bott, A.: On the influence of the physico-chemical properties of aerosols on the life cycle of radiation fogs, Boundary-Layer Meteorol., 56, 1–31, 1991.

Bott, A. and Trautmann, T.: PAFOG—a new efficient forecast model of radiation fog and low-level stratiform clouds, Atmos. Res., 64, 191–203, 2002.

Bougeault, P.: Modeling the trade-wind cumulus boundary layer. Part I: Testing the ensemble cloud relations against numerical data, J. Atmos. Sci., 38, 2414–2428, 1981.

Boutle, I., Price, J., Kudzotsa, I., Kokkola, H., and Romakkaniemi, S.: Aerosol-fog interaction and the transition to well-mixed radiation fog, Atmos. Chem. Phys., 18, 7827–7840, 2018.

Clark, T. L.: Numerical modeling of the dynamics and microphysics of warm cumulus convection, J. Atmos. Sci., 30, 857–878, 1973.

Clough, S. A., Shephard, M. W., Mlawer, E. J., Delamere, J. S., Iacono, M. J., Cady-Pereira, K., Boukabara, S., and Brown, P. D.: Atmospheric radiative transfer modeling: A summary of the AER codes, Short Communication, J. Quant. Spectrosc. Radiat. Transfer, 91, 233–244, 2005.

Cohard, J.-M. and Pinty, J.-P.: A comprehensive two-moment warm microphysical bulk scheme. I: Description and tests, Quart. J. Roy. Meteor. Soc., 126, 1815–1842, 2000.

Cohard, J.-M., Pinty, J.-P., and Bedos, C.: Extending Twomey's analytical estimate of nucleated cloud droplet concentrations from CCN spectra, J. Atmos. Sci., 55, 3348–3357, 1998.

Cohard, J.-M., Pinty, J.-P., and Suhre, K.: On the parameterization of activation spectra from cloud condensation nuclei microphysical properties, J. Geophys. Res. Atmos., 105, 11 753–11 766, 2000.

Deardorff, J. W.: Stratocumulus-capped mixed layers derived from a three-dimensional model, Boundary-Layer Meteorol., 18, 495–527, 1980.

Geoffroy, O., Brenguier, J.-L., and Sandu, I.: Relationship between drizzle rate, liquid water path and droplet concentration at the scale of a stratocumulus cloud system, Atmos. Chem. Phys., 8, 4641–4654, 2008.

Geoffroy, O., Brenguier, J.-L., and Burnet, F.: Parametric representation of the cloud droplet spectra for LES warm bulk microphysical schemes, Atmos. Chem. Phys., 10, 4835–4848, 2010.

Grabowski, W. W. and Morrison, H.: Toward the mitigation of spurious cloud-edge supersaturation in cloud models, Mon. Weather Rev., 136, 1224–1234, 2008.

Gultepe, I., Müller, M. D., and Boybeyi, Z.: A new visibility parameterization for warm-fog applications in numerical weather prediction models, J. Appl. Meteor. Climatol., 45, 1469–1480, 2006.

Gultepe, I., Tardif, R., Michaelides, S., Cermak, J., Bott, A., Bendix, J., Müller, M. D., Pagowski, M., Hansen, B., Ellrod, G., et al.: Fog research: A review of past achievements and future perspectives, in: Fog and Boundary Layer Clouds: Fog Visibility and Forecasting, pp. 1121–1159, Springer, 2007.

Gultepe, I., Hansen, B., Cober, S., Pearson, G., Milbrandt, J., Platnick, S., Taylor, P., Gordon, M., and Oakley, J.: The fog remote sensing and modeling field project, Bull. Amer. Meteor. Soc., 90, 341–359, 2009.

Haeffelin, M., Bergot, T., Elias, T., Tardif, R., Carrer, D., Chazette, P., Colomb, M., Drobinski, P., Dupont, E., Dupont, J.-C., et al.: PARIS-FOG: shedding new light on fog physical processes, Bull. Amer. Meteor. Soc., 91, 767–783, 2010.

Hammer, E., Gysel, M., Roberts, G., Elias, T., Hofer, J., Hoyle, C., Bukowiecki, N., Dupont, J.-C., Burnet, F., Baltensperger, U., et al.: Size-dependent particle activation properties in fog during the ParisFog 2012/13 field campaign, Atmos. Chem. Phys., 14, 10 517–10 533, 2014.

Heus, T., Van Heerwaarden, C., Jonker, H. J., Siebesma, A. P., Axelsen, S., Van Den Dries, K., Geoffroy, O., Moene, A., Pino, D., De Roode, S., et al.: Formulation of the Dutch Atmospheric Large-Eddy Simulation (DALES) and overview of its applications, Geosci. Model Dev., 3, 415, 2010.

Khairoutdinov, M. and Kogan, Y.: A new cloud physics parameterization in a large-eddy simulation model of marine stratocumulus, Mon. Weather Rev., 128, 229–243, 2000.

Khvorostyanov, V. I. and Curry, J. A.: Aerosol size spectra and CCN activity spectra: Reconciling the lognormal, algebraic, and power laws, J. Geophys. Res. Atmos., 111, 2006.

Kokkola, H., Korhonen, H., Lehtinen, K., Makkonen, R., Asmi, A., Järvenoja, S., Anttila, T., Partanen, A.-I., Kulmala, M., Järvinen, H., et al.: SALSA–a Sectional Aerosol module for Large Scale Applications, Atmos. Chem. Phys., 8, 2469–2483, 2008.

Lebo, Z. J., Morrison, H., and Seinfeld, J. H.: Are simulated aerosol-induced effects on deep convective clouds strongly dependent on saturation adjustment?, Atmos. Chem. Phys., 12, 9941–9964, 2012.

Maalick, Z., Kühn, T., Korhonen, H., Kokkola, H., Laaksonen, A., and Romakkaniemi, S.: Effect of aerosol concentration and absorbing aerosol on the radiation fog life cycle, Atmos. Environ., 133, 26–33, 2016.

Maronga, B. and Bosveld, F.: Key parameters for the life cycle of nocturnal radiation fog: a comprehensive large-eddy simulation study, Quart. J. Roy. Meteor. Soc., 2017.

Maronga, B., Gryschka, M., Heinze, R., Hoffmann, F., Kanani-Sühring, F., Keck, M., Ketelsen, K., Letzel, M. O., Sühring, M., and Raasch, S.: The Parallelized Large-Eddy Simulation Model (PALM) version 4.0 for atmospheric and oceanic flows: model formulation, recent developments, and future perspectives, Geosci. Model Dev., 2015.

Mazoyer, M., Lac, C., Thouron, O., Bergot, T., Masson, V., and Musson-Genon, L.: Large eddy simulation of radiation fog: impact of dynamics on the fog life cycle, Atmos. Chem. Phys., 17, 13 017, 2017.

Mensah, A., Holzinger, R., Otjes, R., Trimborn, A., Mentel, T. F., Brink, H. t., Henzing, B., and Kiendler-Scharr, A.: Aerosol chemical composition at Cabauw, The Netherlands as observed in two intensive periods in May 2008 and March 2009, Atmos. Chem. Phys., 12, 4723–4742, 2012.

Morrison, H. and Grabowski, W. W.: Comparison of bulk and bin warm-rain microphysics models using a kinematic framework, J. Atmos. Sci., 64, 2839–2861, 2007.

Morrison, H. and Grabowski, W. W.: Modeling supersaturation and subgrid-scale mixing with two-moment bulk warm microphysics, J. Atmos. Sci., 65, 792–812, 2008.

Nakanishi, M.: Large-eddy simulation of radiation fog, Boundary-Layer Meteorol., 94, 461–493, 2000.

Pruppacher, H. R. and Klett, J. D.: Microphysics of clouds and precipitation, Kluwer Academic Publishers, Dordrecht, Netherlands, 2nd revised edn., 1997.

Seifert, A. and Beheng, K. D.: A double-moment parameterization for simulating autoconversion, accretion and selfcollection, Atmos. Res., 59, 265–281, 2001.

Seifert, A., Khain, A., Pokrovsky, A., and Beheng, K. D.: A comparison of spectral bin and two-moment bulk mixed-phase cloud microphysics, Atmos. Res., 80, 46–66, 2006.

Shima, S., Kusano, K., Kawano, A., Sugiyama, T., and Kawahara, S.: The super-droplet method for the numerical simulation of clouds and precipitation: A particle-based and probabilistic microphysics model coupled with a non-hydrostatic model, Quart. J. Roy. Meteor. Soc., 135, 1307–1320, 2009.

Stolaki, S., Haeffelin, M., Lac, C., Dupont, J.-C., Elias, T., and Masson, V.: Influence of aerosols on the life cycle of a radiation fog event. A numerical and observational study, Atmos. Res., 151, 146–161, 2015.

Thouron, O., Brenguier, J.-L., and Burnet, F.: Supersaturation calculation in large eddy simulation models for prediction of the droplet number concentration, Geosci. Model Dev., 5, 761–772, 2012.

Twomey, S.: The nuclei of natural cloud formation part II: The supersaturation in natural clouds and the variation of cloud droplet concentration, Pure Appl. Geophys., 43, 243–249, 1959.

Wicker, L. J. and Skamarock, W. C.: Time-splitting methods for elastic models using forward time schemes, Mon. Weather Rev., 130, 2088–2097, 2002.

Williamson, J.: Low-storage runge-kutta schemes, J. Comput. Phys., 35, 48–56, 1980.

Zhang, X., Musson-Genon, L., Dupont, E., Milliez, M., and Carissimo, B.: On the influence of a simple microphysics parametrization on radiation fog modelling: A case study during parisfog, Boundary-Layer Meteorol., 151, 293–315, 2014.